THESIS

MIXING OF SCALARS IN TURBULENT FLOWS USING DIRECT NUMERICAL SIMULATIONS

Submitted by

Ajithshanthar Nithianantham

Department of Civil and Environmental Engineering

In partial fulfillment of the requirements

For the Degree of Master of Science

Colorado State University

Fort Collins, Colorado

Fall 2015

Master's Committee:

Advisor: S. Karan Venayagamoorthy

Pierre Julien
Hiroshi Sakurai

ABSTRACT

MIXING OF SCALARS IN TURBULENT FLOWS USING DIRECT NUMERICAL SIMULATIONS

The research presented in this thesis focuses on scalar mixing in unstratified (neutral) flows and stably stratified flows using Direct Numerical Simulations (DNS). Such flows are ubiquitous in natural flows such as rivers, estuaries, oceans and the atmosphere. First, a detailed study was performed to investigate the effect of varying Schmidt numbers (*Sc*) on turbulent mixing of a passive scalar in a stationary homogeneous unstratified flow using forced DNS. A total of 6 simulations were performed for $0.1 \leq Sc < 3$. Qualitative and quantitative results of the flow field and the passive scalar fields are presented and discussed. The effect of the Schmidt number on the turbulent mixing was found to be negligible and becomes important (as it should) only when mixing occurs under laminar flow conditions.

Using a model proposed by Venayagamoorthy and Stretch in 2006 for the turbulent diascalar diffusivity as a basis, a practical (and new) model for quantifying the turbulent diascalar diffusivity is proposed as $K_S = 1.1\,\gamma'\,L_T\,k^{1/2}$, where L_T is defined as the Thorpe length scale, k is the turbulent kinetic energy and γ' is one-half of the mechanical to scalar time scale ratio, which was shown by previous researchers to be approximately 0.7. The novelty of the proposed model lies in the use of L_T, which is a widely used length scale in stably stratified flows (almost exclusively used in oceanography), for quantifying turbulent mixing in unstratified flows. L_T can be readily obtained in the field using a Conductivity, Temperature and Depth (CTD) profiler or obtained from density fields in a numerical model. The turbulent kinetic energy is mostly contained

in the large scales of the flow field and hence can be measured in the field using devices such as an Acoustic Doppler Current Profiler (ADCP) or modeled in numerical simulations. Comparisons using DNS data show remarkably good agreement between the predicted and exact diffusivities.

Finally, the suitability of the proposed model for stably stratified flows was explored for varying degrees of stratification ranging from mildly stable flow conditions to strongly stable conditions. In stably stratified flows, density variations of the fluid dynamically affect the flow field and hence the density acts as what is widely known as an active scalar. Under strongly stable conditions, the DNS results indicate an inverse relationship between the Thorpe scale L_T and kinetic energy length scale $L_{k\varepsilon}$, which is different to the direct (almost one to one correspondence) relationship that was found for unstratified flows. Hence, in order to account for this difference, a modified turbulent diascalar diffusivity model was proposed as $K_d = 13\,\gamma'\,{L_T}^3\,k^{1/2}$. It must be noted that this modified model while dimensionally inconsistent (due to the inverse relationship between the length scales), provides reasonable quantitative estimates of the diffusivity under stably stratified flow conditions.

The models proposed in this study require further (extensive) testing under higher Reynolds number flow conditions. If shown to be valid, they would be widely useful for quantifying turbulent mixing using field measurements of large scale quantities (i.e. L_T and k) as well as a simple and improved turbulence closure scheme.

ACKNOWLEDGEMENTS

Foremost, I would like to thank my adviser, mentor Dr. Karan, for all his continuous support and help in all the ways in my academic life and otherwise. His patience, enthusiasm, immense knowledge and confidence in my abilities kept me motivated to achieve my goal of graduating with my master's degree. I couldn't have imagined having a better advisor and mentor for my master's study. He is also a major reason why we are planning to publish an article in a journal, an accomplishment I can always be proud of.

Next I wish to express gratitude to my parents for giving birth to me at the first place and supporting me spiritually throughout my life. Your never-ending love and care as I am removed far away from you gave me the mindset that I needed to be successful. Thank you for always being there for me and always being willing to lend a hand.

My sincere thanks also go to Simon Schaad, former master student of Dr. Karan. His significant work on numerical simulations and Matlab coding gave me guidance to achieve successful DNS simulations and data post processing. I thank my fellow lab mates in the Environmental Fluid Mechanics Research Group at CSU – Farid Karimpour, Jordan Wilson, Ben Mater, Amrapalli Garanaik, Oladapo Aseperi, Jeremy Carlston and Jian Zhou - were all obliging when I had questions or needed help.

Finally I would like to acknowledge and thank Prof. Julien and Dr. Sakurai for taking time out of their busy schedules to serve on my thesis committee. Your insight, suggestions, and comments are truly appreciated.

TABLE OF CONTENTS

LIST OF FIGURES

CHAPTER 1

INTRODUCTION

1.1 Introduction

Turbulent flows are ubiquitous in natural and engineering systems involving liquids and gases. Turbulent flows are generally irregular, chaotic and nonlinear and hence very difficult to predict and model. Examples of turbulent flows in engineering include flow of water in rivers, engineered canals, pipes and flow of air in the atmosphere and engineered systems. A key characteristic of turbulence is enhanced mixing which can be advantageous in certain situations such as when rapid dilution of a substance is desirable and can be detrimental when an opposite scenario that requires little to no mixing is required.

Natural flows can be unstratified where the density of the fluid is constant across the whole fluid column (i.e. in well mixed rivers and neutral atmospheric boundary layer) or stratified where the density changes with depth. The density (which is a scalar quantity) can be considered to be passive in the former case (unstratified flows) in that it does not dynamically influence the momentum field. In other words, it passively mixes driven by the resultant turbulent velocity field without any feedback on the driving velocity field. On the other hand, in a stably stratified fluid (i.e. where density increases with depth e.g. in the oceans), the density is considered as an active scalar in the sense that it dynamically influences the momentum field through buoyancy effects. Hence, mixing of scalars in these two types of conditions are different and appropriate considerations for these differences must be given in the development of turbulent mixing model for mixing. However, it is clear that despite numerous studies on scalar mixing, there are many unresolved issues concerning both the fundamental aspects of turbulent mixing in such flows as

more practical issues related to modeling of such flows for solving many important environmental flow problems.

The work presented in this thesis focuses on mixing of scalars in both unstratified flows and stratified flows. Mixing of a passive scalar is studied in unstratified flows using forced Direct Numerical Solution (DNS). Besides providing a direct solution to the highly nonlinear Navier-Stokes equations that govern the motion of fluid flow without recourse to turbulence closure models, DNS also provides the ability for the researcher to probe the full three-dimensional flow fields.

In what follows, a brief outline of the main objectives and the layout of the thesis are presented.

1.2 Objectives

The main objectives of this study are as follows:

1) To perform analyses of homogeneous, unstratified turbulent flow with a range of Schmidt numbers using forced DNS in order to investigate the molecular effects on turbulent mixing in such flows.
2) To develop a turbulent scalar diffusivity model for passive scalar mixing in unstratified flows that is practically useful.
3) To develop a turbulent scalar diffusivity model for active scalar mixing in stably stratified flows that is also practically useful.

1.3 Thesis Layout

The contents of this thesis have been arranged into four further chapters. Chapter 2 presents a brief literature review including important governing equations as well a discussion on passive scalar and active scalar mixing. Basic fluid mechanics theory on turbulence related to stratified

and unstratified flow are presented; specifically definitions of important parameters, the governing equations, relevant scales, and important non-dimensional parameters are provided. Relevant review of previous work done on scalar mixing discussed.

In Chapter 3, a parametric study of passive scalar mixing in homogeneous unstratified flows with different Schmidt numbers using DNS is reported. Details of simulation setup and numerical methods are briefly discussed. The DNS results for the energetics and scalar properties are discussed. Visualizations of vorticity, enstrophy and density fields are presented to provide qualitative description of coherent turbulent structures of the flow and scalar fields. Finally, an innovative attempt is made develop a model for scalar mixing in unstratified flow.

An extension of the research presented in Chapter 3 pertaining to mixing is made to stably stratified flows in chapter 4. The applicability of a proposed scalar diffusivity model that is extensively discussed in chapter 3 is tested and refined for the prediction of active scalar mixing in stably stratified flows. Chapter 5 concludes this thesis where a summary of the work done is provided together with the main finding. Some recommendations for future work are also provided in Chapter 5.

CHAPTER 2

LITERATURE REVIEW

2.1 Introduction

Turbulent flows are characterized by enhanced mixing and thus help to distribute and transport many substances such as contaminants and nutrients in natural flows as well as engineered flows (e.g. in combustion engines). Thus, the subject of scalar mixing in turbulent flows has received much attention over the years using a myriad of approaches that combine theory, experiments and numerical simulations. In environmental flows, the density of the fluid could be either constant over the whole water or air column (e.g. in river flows, the water is more or less homogeneous and the density is assumed to be constant) or it could vary with depth (e.g. summer conditions in a lake will result in a two-layer system where the upper layer will be warm and well mixed and the lower layer will be cooler with a thermocline separating the two layers). Understanding and modeling mixing of scalars in environmental flows is important for obvious reasons. Here, the salient features of turbulent flows are presented.

In what follows, first a brief overview of the governing equations of fluid motion and scalar transport are discussed in Sec. 2.2. This is followed by a discussion on the basic non-dimensional parameters that are relevant to this research in Sec.2.3. Turbulent length and time scales are discussed in Sec.2.4 and turbulent diffusivity parameterizations are reviewed in Sec. 2.5.

2.2 Equations of motion

Behavior of fluid motion can be described by the governing conservation principles of momentum, mass and energy.

2.2.1 Governing Equations

In unstratified turbulent flows, density does not play a dynamic role on the fluid motion since it is constant. Hence, only the conservation of momentum principle which leads to the well-known Navier-Stokes equations in fluids and the conservation of mass principle (resulting in the continuity equation) are sufficient to describe the flow.

2.2.1.1 The Navier-Stokes Equations

The Navier-Stokes equations for an unstratified flow is given by

$$\rho \frac{\partial u}{\partial t} + \rho(u.\nabla \mathrm{u}) = -\nabla \mathrm{P} + \mu \nabla^2 u, \tag{2.1}$$

where, ρ is the (constant) density of the fluid, **u** is the velocity vector (with components u, v, and w, respectively), ∇P is the pressure gradient and μ is the molecular dynamic viscosity. Eq.2.1 can be rewritten with the total derivative notation $D()/Dt = \partial()/\partial t + \mathbf{u}.\nabla()$ as follows

$$\rho \frac{Du}{Dt} = -\nabla P + \mu \nabla^2 u, \tag{2.2}$$

For stratified flows, the buoyancy effects are taken into account because of the variation of density. Hence, Eq.2.2 can be rewritten by including the force of gravity ($\boldsymbol{g}$) tern to get

$$\rho \frac{Du}{Dt} = -\nabla P + \mu \nabla^2 u + \rho g, \tag{2.3}$$

Equation (2.3) can be further simplified using the Boussinesq approximation which is based on the assumption that variations in density have negligible effect on the inertial terms. The assumption formally requires that the density variations are small (i.e. $\rho'/\rho_o \ll 1$) and can be

shown to be valid for low Mach number flows. Hence, using the Bousinesq assumption, the momentum equations are given by

$$\frac{Du}{Dt} = -\frac{1}{\rho_o}\nabla \mathrm{p} + \nu\nabla^2 u + \frac{\rho'}{\rho_o} g, \tag{2.4}$$

where, ρ' is the density fluctuation from the background mean density (ρ_o).

2.2.1.2 Continuity Equation

The principle of conservation of mass leads to the continuity equation given by

$$\frac{\partial \rho}{\partial t} + \nabla.(\rho u) = 0, \tag{2.5}$$

Using the total Derivative notation, the above equation can be rearranged into

$$\frac{D\rho}{Dt} + \rho.\nabla(u) = 0, \tag{2.6}$$

Eq. (2.6) simplifies further for an incompressible fluid to a divergence free velocity field given by

$$\nabla.u = 0, \tag{2.7}$$

2.2.1.3 Scalar Transport Equation

The ratio of the kinematic viscosity (ν), of a fluid to the molecular diffusivity (κ) of a scalar quantity is either called the Schmidt number *Sc* (for mass diffusivity) or Prandtl number *Pr* (for heat diffusivity) as

$$Sc\ (Pr) = \frac{\nu}{\kappa}, \tag{2.8}$$

The transport equation for scalar fluctuation θ' is given by

$$\frac{\partial \theta'}{\partial t} + u.\nabla\theta' = \kappa\nabla^2\theta', \tag{2.9}$$

where u is the velocity vector obtained from the Navier-Stokes equations. Eq.2.9 can be simplified using total derivative material notation as.

$$\frac{D\theta'}{Dt} = \kappa\nabla^2\theta', \tag{2.10}$$

2.3 Basic Parameters of Turbulent flow

There are several important non-dimensional parameters that are commonly used for describing turbulent flows and stratification. The key parameters that will be used throughout this thesis are defined next.

2.3.1 Reynolds Number

Reynolds number (*Re*) is a key parameter in fluid mechanics. It is essentially a ratio of inertial to viscous forces and is used to characterize whether a flow is laminar or turbulent. In DNS simulations that are initialized with some energy input, an initial turbulent Reynolds number is usually defined as

$$Re_o = \frac{U_o L_o}{\nu}, \tag{2.11}$$

Where, ν is the kinematic viscosity of the flow. U_o and L_o are the initial velocity and length scales of the flow. Another commonly used Reynolds number that is defined using the turbulent length scale *L* and turbulent kinetic energy *k* of the flow is the turbulent Reynolds number expressed in Eq. (2.12).

$$Re_L = \frac{k^{1/2}L}{\nu}, \tag{2.12}$$

$$Re_\lambda = \frac{u_{rms}L_\lambda}{\nu}, \tag{2.13}$$

Using Taylor microscale $L_\lambda = \sqrt{5\nu\langle u_i u_i\rangle/\varepsilon}$, a statistical quantity, a Taylor Reynolds number can be defined as shown in Eq. (2.13).

2.3.2 Richardson Number

The Richardson Number *Ri*, a non-dimensional parameter that is defined as the ratio of the buoyancy forces to inertial forces in a turbulent flow. It expresses the strength of the stratification of the flow in terms of the buoyancy frequency *N* and initial eddy turnover time scale $T_o = {L_o}/{U_o}$. *Ri* is given as

$$Ri_o = \left[\frac{NL_o}{U_o}\right]^2, \tag{2.14}$$

where the buoyancy frequency *N* is defined as

$$N = \left[-\frac{g}{\rho_o}\left(\frac{\partial\bar{\rho}}{\partial z}\right)\right]^{1/2}, \tag{2.15}$$

The buoyancy frequency *N* is also called as the Brunt-$Väisälä$ frequency. Here, g is the acceleration due to gravity and $\frac{\partial\bar{\rho}}{\partial z}$ is the mean density gradient in the vertical direction.

2.3.3 Schmidt (or Prandtl) and Peclet Number

The Schmidt (or Prandtl) number *Sc* (*Pr*) measures the ratio of kinematic viscosity (of the fluid) to molecular diffusivity (of the scalar) effects in the flow as previously defined in Eq.(2.8). The Peclet Number can be defined as a ratio between the rates of advection to diffusion in a turbulent flow.

$$Pe = \frac{Advection}{Diffusion} = \frac{U_o L_o}{\kappa}, \tag{2.16}$$

Where U_o and L_o are the initial velocity and length scales of the flow, and κ is molecular diffusivity. Also it can be rearranged in terms of a Reynolds number *Re* and the Schmidt number *Sc* for mass transfer as follows

$$Pe = Re.Sc, \tag{2.17}$$

2.4 Length and Time Scales

Turbulent flows are characterized by a large range of length and time scales. These scales range from large scales that are defined by the forcing of the flow field as well as the geometry to the small scales which are characteristic of the dissipative scales. The small scales at which molecular viscosity acts to dissipate the kinetic energy are called the Kolmogorov scales in a turbulent flow. However, the dissipative scales associated with scalars in turbulent flows maybe finer or larger than the Kolmogorov length scales depending on the *Sc* or *Pr*. These scales are discussed in sections 2.4.2 and 2.4.3.

2.4.1 Energy cascade and Kolmogorov Scales

An early and commonly adapted notion is the energy cascade first put forth by Richardson (1922). A turbulent flow can be considered to consist of eddies of different sizes ranging from large eddies to small eddies. The large eddies (which extract their energy from the mean flow) are dominated by inertial forces and are presumably unaffected by viscous effects. However, due their high energy content, such large eddies are unstable and hence transfer their energy to smaller eddies which in turn undergo a similar process and spurn even smaller eddies. This process continues till the local Reynolds number of the smallest eddies is small enough (of the order of 1),

for viscosity to stabilize the eddy and dissipate its turbulent kinetic energy effectively (Pope, 2010). The energy cascade idea was summarized as a poem by Richardson as follows:

Big whorls have little whorls,
Which feed on their velocity;
And little whorls have lesser whorls,
And so on to viscosity

-Lewis F. Richardson

Andrey N. Kolmogorov, a Soviet mathematician is widely credited with putting forth the first set of ideas towards formalizing a universal theory of turbulence in 1941. These set of ideas are captured through the famous 'Kolmogorov's hypotheses. A key hypothesis of local isotropy states that: the large eddies are anisotropic and while the small eddies are isotropic at the dissipative scales. Kolmogorov's ***First similarity hypothesis*** is based on the argument that small scale turbulent motions in the universal equilibrium range are uniquely determined by kinematic viscosity *v*, and dissipation rate ε_k. Using these determining parameters, unique length, velocity and time scales can be constructed from dimensional analysis. These three scales are considered as the so called-smallest scales of motion in turbulent flows. The Kolmogorov's length (L_η), time (τ_η), and velocity (u_η) scales are define as follows:

$$L_\eta = (\nu^3/\varepsilon)^{1/4}, \tag{2.18}$$

$$u_\eta = (\varepsilon\nu)^{1/4}, \tag{2.19}$$

$$\tau_\eta = (\nu/\varepsilon)^{1/2}, \tag{2.20}$$

2.4.2 Obukhov-Corrsin and Batchelor Scales

Obukhov (1949) and Corrsin (1951) were the first to propose extensions of Kolmogorov's phenomenology to passive scalars. The scalar dissipative regimes can be divided in two demarcated by *Sc*=1. The two regimes are known as inertial-diffusive range and viscous-

convective range when *Sc*<1 and *Sc*>1, respectively (see Fig.2.1). Scalar spectrums in these regions can be expressed as shown in Eq.2.21 and 2.22.

$$E_\rho(K) = C_{OC}\,\varepsilon_\rho\,\bar{\varepsilon}^{(-\frac{1}{3})}\,K^{(-\frac{5}{3})}, \qquad for\ 1/L \ll K \ll 1/L_{OC} \tag{2.21}$$

$$E_\rho(K) = C_B\,\varepsilon_\rho\,(\nu/\bar{\varepsilon})^{(\frac{1}{2})}\,K^{(-1)}, \qquad for\ 1/L_\eta \ll K \ll 1/L_B \tag{2.22}$$

where, C_{OC} is known as the Obukhov-Corrsin constant, C_B is the Batchelor constant, ε_ρ is scalar dissipation rate, $\bar{\varepsilon}$ is the mean rate of energy dissipation rate per unit mass and K is wavenumber.

When *Sc*<1, range of scales $L \gg 1/K \gg 1/L_{OC}$, which shows that neither molecular viscosity nor molecular diffusion is important. Thus, it is called inertial-convective range. For the case when *Sc*≥1, the scale $L_B = L_\eta Sc^{-1/2}$ is smaller than L_η. Therefore a viscous-convective range may form where viscosity is important but not the diffusivity.

The Batchelor scale L_B (Batchelor, 1959) is a length scale where the molecular diffusion of a scalar is dominated by energy dissipation. It is defined as

$$L_B = \left(\frac{k^2\nu}{\varepsilon}\right)^{1/4}, \tag{2.23}$$

The Batchelor scale and Obukhov-Corrsin scale can be related with Kolmogorov length scale in terms of *Sc* as follows

$$L_B = \frac{L_\eta}{Sc^{1/2}}, \tag{2.24}$$

$$L_{OC} = \frac{L_\eta}{Sc^{3/4}}, \tag{2.25}$$

Hence, when *Sc* >1, L_B is smaller than the Kolmogorov scale.

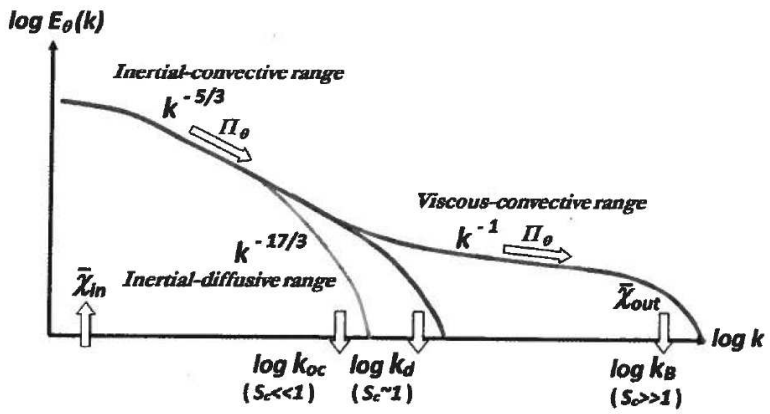

Figure 2.1: Schematic sketch of spectrum of passive scalar variance. Scalar fluctuations are injected at low wave numbers at rate $\bar{\chi}_{in}$and transferred to high wave numbers with the mean flux $\pi_\theta$and then smeared by the molecular diffusivity at the rate $\bar{\chi}_{out}$. (Gotoh and Yeung, 2012).

2.4.3 Thorpe and Ellison length scales

The Thorpe displacement d' is the vertical distance a particle must travel back to a position along a gravitationally stable density profile. The gravitationally stable density profile is calculated by monotonically sorting the density profile. The Thorpe scale L_T is the root-mean square of non-zero d'along a vertical profile and provides a measure of the size of vertical overturns (Thorpe, 1977).

The Ellison scale L_E is an additional measure of the maximum vertical displacement, given a background density profile and a turbulent intensity estimated by $1/2\overline{(\rho'^2)}$.

$$L_E = \overline{(\rho'^2)}^{1/2} / |\partial\bar{\rho}/\partial z| \,, \tag{2.26}$$

If sorted density profile is exactly equal to $\partial\bar{\rho}/\partial z$, then L_E is exactly equal to L_T. However, a relationship of $L_T = 0.8\ L_E$ was proposed by Itsweire et al. (1993) for stably stratified shear flows as shown in Fig.2.2.

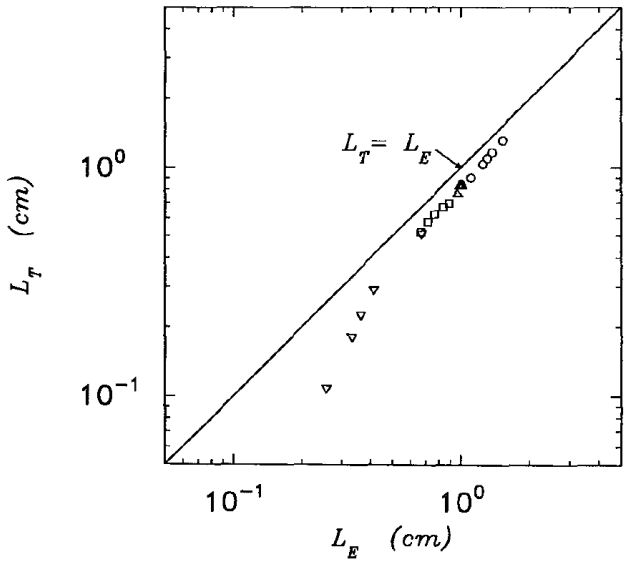

Figure 2.2: relationship between Thorpe and Ellison length scales (Itsweire et al. 1993).

2.5 Diapycnal diffusivity

The diapycnal diffusivity is a measure of the irreversible mixing in a density stratified flow. Venayagamoorthy and Stretch (2006) proposed a model to define the turbulent diffusivity in terms of Ellison length scale and turbulent time scale as

$$K_d = \gamma' \frac{{L_E}^2}{T_L}, \tag{2.27}$$

where, L_E is the Ellison 'overturning' length scale, T_L is turbulent time scale and γ' is one-half of the ratio of the mechanical-to-scalar time scale given by

$$\gamma' = \frac{1}{2} \frac{\varepsilon_\rho T_L}{\overline{(\rho'^2)}/2}, \tag{2.28}$$

where ε_ρ scalar dissipation, T_L is the turbulent time scale ($T_L = k/\varepsilon$) and ρ' is mean scalar fluctuation. Fig.2.3 is a plot of the non-dimensional diapycnal diffusivity (K_S/κ) with turbulent Peclet number ($Pe_t = {L_E}^2/T_L\kappa$) for a different of datasets taken from a study conducted by Stretch and Venayagamoorthy (2010) to assess the validity of the diapycnal diffusivity they proposed as shown in Eq. (2.27).

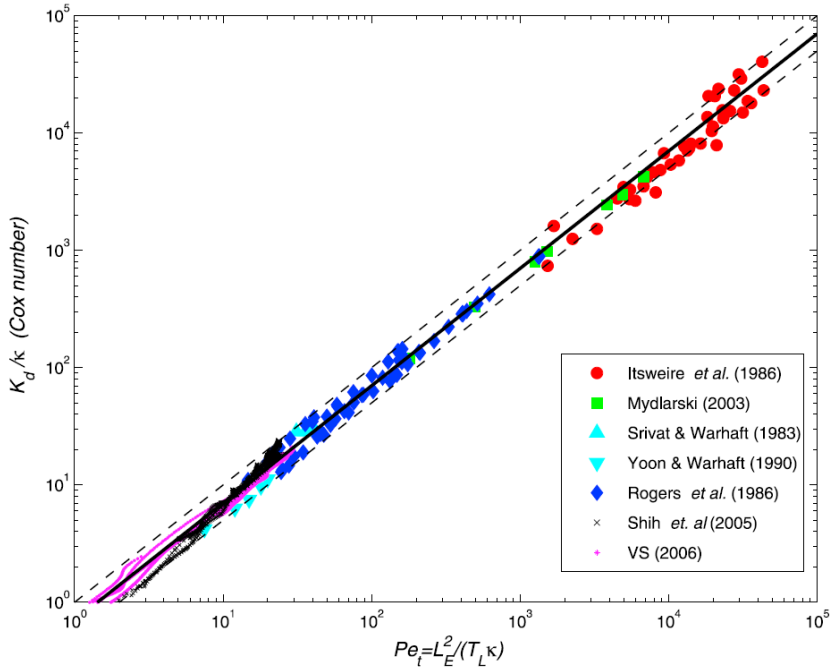

Figure 2.3: non-dimensional diapycnal diffusivity is plotted with turbulent Peclet number (from Stretch and Venayagamoorthy 2010).

2.6 Conclusions

In this short chapter, an overview of the key equations and parameters was provided to set the stage for the research study presented in the next two chapters.

CHAPTER 3

TURBULENT MIXING OF PASSIVE SCALARS

3.1 Introduction

This chapter presents results from a detailed study was performed to investigate the effect of varying Schmidt numbers (*Sc*) on turbulent mixing of a passive scalar in a stationary homogeneous unstratified flow using forced DNS. Here, a passive scalar by definition is a scalar quantity that does not affect the flow (momentum) field dynamically. Examples of such scalars include a dissolved pollutant such as Nitrogen or Chlorine that is transported in a turbulent flow. The dissipation and mixing of passive scalars occurs at small scales which besides the Reynolds number, may also be influenced by the Schmidt number (*Sc*). The *Sc* can vary widely by several orders of magnitude ranging from 10^{-3} in liquid metals to order unity in gaseous flames to 10^{3} or higher in organic mixtures and biological fluids (Yeung *et al*., 2002). However, to date, it is not clear what the effect of *Sc* is in high Reynolds number turbulent flows, especially pertaining to the prediction of turbulent mixing of scalars in such flow.

In what follows in this chapter, first a formal problem statement is stated in Sec. 32. This is followed in Sec.3.3 by a discussion on the DNS formulation and numerical resolution issues. DNS results of the energetics and dynamics of the flow field are presented in Sec 3.4 for Sc =1, noting that for passive scalars, the velocity fields for different *Sc* simulations are identical. In Sec 3.5, DNS results for scalar dissipation and fluxes are presented for $0.1 \leq Sc < 3$. The coherent structures of both the flow field and scalar are qualitatively visualized in three-dimensional space in Sec. 3.6. Finally, a practical (and new) model for quantifying the turbulent diascalar diffusivity is presented in Sec. 3.7.

3.2 Problem Statement

The overarching question that primarily motivates the work presented in this chapter is "Does the turbulent mixing of a passive scalar in a homogeneous, unstratified turbulent flow depend on the molecular diffusivity (specified by different Schmidt number *Sc*)?"

An associated and practical question that follows pertains to whether a unifying model can be proposed for quantifying the turbulent diascalar diffusivity of passive scalars in turbulent flows?

It should be noted that it is very challenging to obtain conclusive and elegant answers to both of the above questions due to in part the complexities associated with turbulent flows and also the constraints inherent in the tools such as DNS and experiments that are used to study such flows. However, an attempt to answer these questions is made in this study using DNS simulations for varying *Sc* numbers.

3.3 Direct Numerical Solutions

Direct Numerical Simulation (DNS) is a computational technique for the solving the three-dimensional instantaneous Navier-Stokes (N-S) equations for fluid flow. A turbulent flow is characterized by a large range of length scales ranging from large scales depicted by the geometry of the flow domain to small dissipated scales where most of the turbulent kinetic energy that is produced from the mean flow field at large scales is dissipated. Hence it is very important to solve the N-S equations across this spectrum of length scales in order to investigate the fundamental physics associated with turbulence. Thus DNS has the advantage over other computational fluid dynamics (CFD) methods as it directly solves the flow field up to the smallest scales for a given Reynolds negating the need for a turbulence model that is typically required in all the other CFD techniques.

However the computational cost associated with DNS scales nonlinearly with the Reynolds number. Hence DNS is restricted to low to moderate Reynolds numbers (Pope 2000). Practical environmental flows which are characterized by higher Reynolds numbers require other CFD techniques such as Large Eddy Simulations (LES) and Reynolds Average Navier-Stokes (RANS) simulations which solve some form of the averaged N-S equations in conjunction with a turbulence closure model.

3.3.1 Description of Code

The DNS code used in this current work was pioneered for homogeneous turbulence by Orszag and Patterson (1972) using a pseudo-spectral numerical scheme. The code was extended by Riley et al. (1981) for stratified turbulent flows. The forcing scheme with pseudo spectral method DNS code used in this work for unstratified flow is based on a constant energy input technique using a linear forcing technique (Stretch, personal communication). The code is written in the FORTRAN 77 programming language and executed on a Linux operating system. A pseudo-spectral method is a technique where by the linear terms in the Navier-Stokes equations are evaluated in wavenumber space while the non-linear terms are computed in physical space. Time marching is accomplished using the leap frog scheme in order to achieve second order accuracy at minimal cost. Periodic boundary conditions are applied on all boundaries, which are necessary boundary conditions for spectral schemes (Pope, 2000).

3.3.2 Formulation of DNS

DNS using pseudo spectral numerical method involves the formulation of the flow parameters such as velocity in wavenumber space (*K*) as three dimensional Fourier series for N^3 grid points, where *N* is the number of grids (which is set the same in all three directions). For example, the Fourier series for velocity can be represented as a finite Fourier series as follows

$$u(x,t) = \sum_{K} e^{iK.X}\, \hat{u}(K,t), \tag{3.1}$$

where *K* is the wavenumber is the wavenumber and $\hat{u}$ is the Fourier coefficients. In physical space, the resolving domain is a cube of length of *L* with *N* grid points in each direction. Hence a grid size is $\Delta x = \Delta y = \Delta z = L/N$. Discrete Fourier Transform (DFT) gives a one-to-one mapping between Fourier coefficients and the velocities. (Pope, 2000).

The computational box (*L*) must be large enough to capture the largest scales of the flow while the grid size should be small enough to capture the smallest dissipative scales. The highest wave number K_{max} can be determined in terms of number of grid points *N* and lowest non-zero wavenumber K_o.

$$K_{max} = \frac{\sqrt{2}}{3} K_o N, \tag{3.2}$$

The turbulent Reynolds number Re_L (Eq. 3.3) can be used to illustrate the computational cost associated with DNS. The number of grid points *N* (Eq. 3.4) in each direction is approximately equal the ratio of the turbulent large scale *L* to the Kolmogorov scale L_η (Durbin & Pettersson Reif, 2011) and typically *N* is chosen to be in power of 2 naturally to facilitate computation of Fourier transforms.

$$Re_L = \frac{k^{1/2} L}{\nu} = \frac{k^2}{\varepsilon \nu}, \tag{3.3}$$

$$N \sim \frac{L}{L_\eta} = \frac{k^{3/2}}{\varepsilon}\left(\frac{\varepsilon}{\nu^3}\right)^{1/4} = \left(\frac{k^2}{\varepsilon\nu}\right)^{3/4} = {Re_L}^{3/4}, \tag{3.4}$$

where k is the turbulent kinetic energy and ε is the rate of dissipation of turbulent kinetic energy and ν is the kinematic viscosity.

3.3.2.1 Forcing scheme

A forcing scheme was added to momentum equation in order to obtain a statistically stationary homogeneous velocity field (Eswaran and Pope, 1987). A linear forcing scheme was used for this purpose, where a forcing is introduced in order to maintain a constant turbulent kinetic energy k as a function of time. The turbulent kinetic energy as a function of time is shown in figure 3.1 and is seen to be almost constant for up to three eddy turnover time. Also, it should be noted that the velocity field and hence the associated energetics of the flow field is identical for all the different simulations that were performed for varying Schmidt numbers (i.e. *Sc* = 0.1, 0.2, 0.5, 1, 2 and 3). Through this approach, a statistically stationary homogeneous turbulent field was maintained throughout the duration of the simulations.

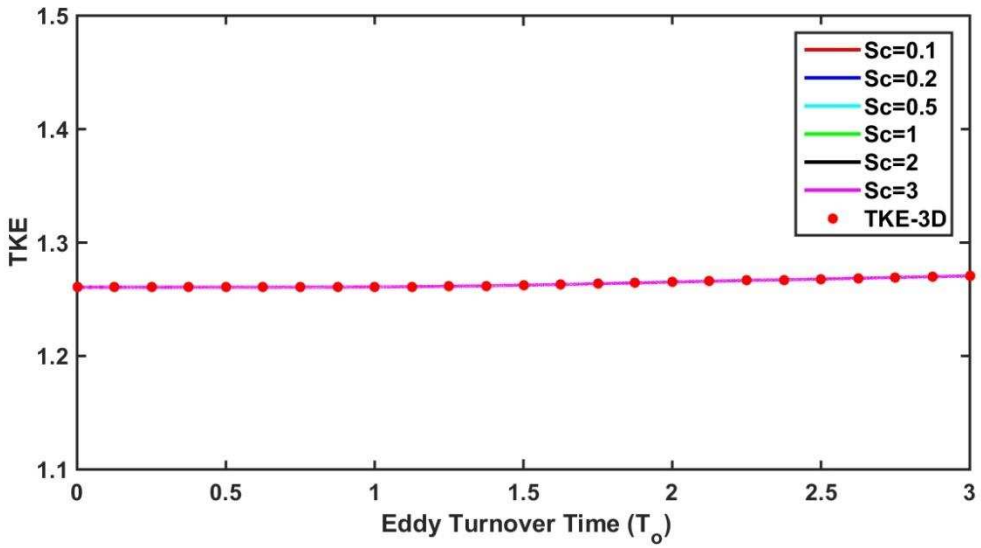

Figure 3.1: Turbulent kinetic energy for unstratified homogeneous flow using DNS at 256^3 grids for *Sc*=0.1, 0.2, 0.5, 1, 2 & 3.

3.3.2.2 Initial Conditions

The simulation was initialized with a Gaussian, Isotropic velocity field using with an energy spectrum function as follows

$$E(K) = C_K U_o^2 L_o^5 K^4 e^{\left(-\frac{1}{2}K^2L^2\right)}, \tag{3.5}$$

where C_κ is the Kolmogorov constant scaling factor, U_o& L_o are initial velocity and length scales. The turbulent Reynolds number Re_L was 625 and the number of grid points N^3 =256^3 for all simulations. DNS at this higher Re_L and number of grid points were checked by Schaad (2012) against the earlier lower resolution DNS study by Venayagamoorthy and Stretch (2006). The initial Richardson number Ri_o was set to zero for all simulations of unstratified turbulence since buoyancy effects are absent in such flows.

Each simulation was performed for up to three eddy turn over time, which is necessary to allow the turbulent flow to reach a stationary state. Hence, the total number of time steps and time step size Δt were determined as 6000 and 0.0005, respectively to achieve three eddy turn time while ensuring numerical stability. The minimum wavenumber (*AKMIN*) was determined as 1 and then increased to 4 to overcome the resolution issues on the results, which are discussed in the next section. Also, the range of Schmidt numbers that were simulated was constrained by the resolution issues.

3.3.3 Resolution issues

All the initial simulations that were performed were done with a minimum wavenumber of 1 (i.e. a dimensional box size equivalent to 2π) in order to allow for the largest possible computational domain which will allow for the largest scales of the flow to evolve in the periodic computational domain. With a minimum wavenumber of 1, each size of the computational cube is

of length 2π, which implies that computational domain is about 6 times larger than the large eddy size (see Fig.3.2).

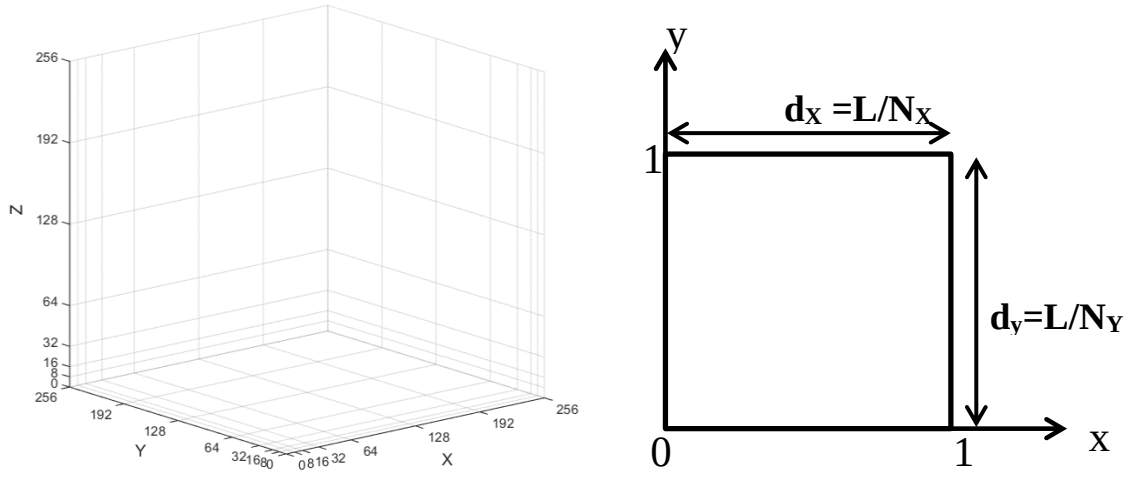

Figure 3.2: a) Three dimensional computational domain with *N*=256 grid points in each direction, b) size of a grid in XY plane

In order to ensure adequate grid resolution, the computational domain must be sufficiently large enough to contain the large scales of the flow while also ensuring that grid size *d (=L/N)* should be sufficiently fine to resolve the smallest scales, which are typically of the order of the Kolmogorov length scale $L_\eta = (\nu^3/\varepsilon)^{1/4}$. Here, ν is the kinematic viscosity and ε is the dissipate rate of turbulent kinetic energy. The Kolmogorov scales were checked to ensure that the grid was sufficiently small in order to confirm that the simulations were adequately resolved. Furthermore, in order to adequately resolve the passive scalar field, the corresponding small length scales commonly known as the Obukhov - Corssin scale (for *Sc* <1) and the Batchelor scale (for *Sc* >1) were also checked against the grid resolution. Fig.3.3 shows all three small length scales together with the grid sizes. As can be seen, clearly, the grid size is not small enough to resolve the small scale motions for all of the Schmidt numbers. Grid sizes are almost 5 times larger than Kolmogorov

scale. Hence it is clear that a smaller computational domain is required to resolve all scale motions of the flow with a total number of grid points of 256^3.

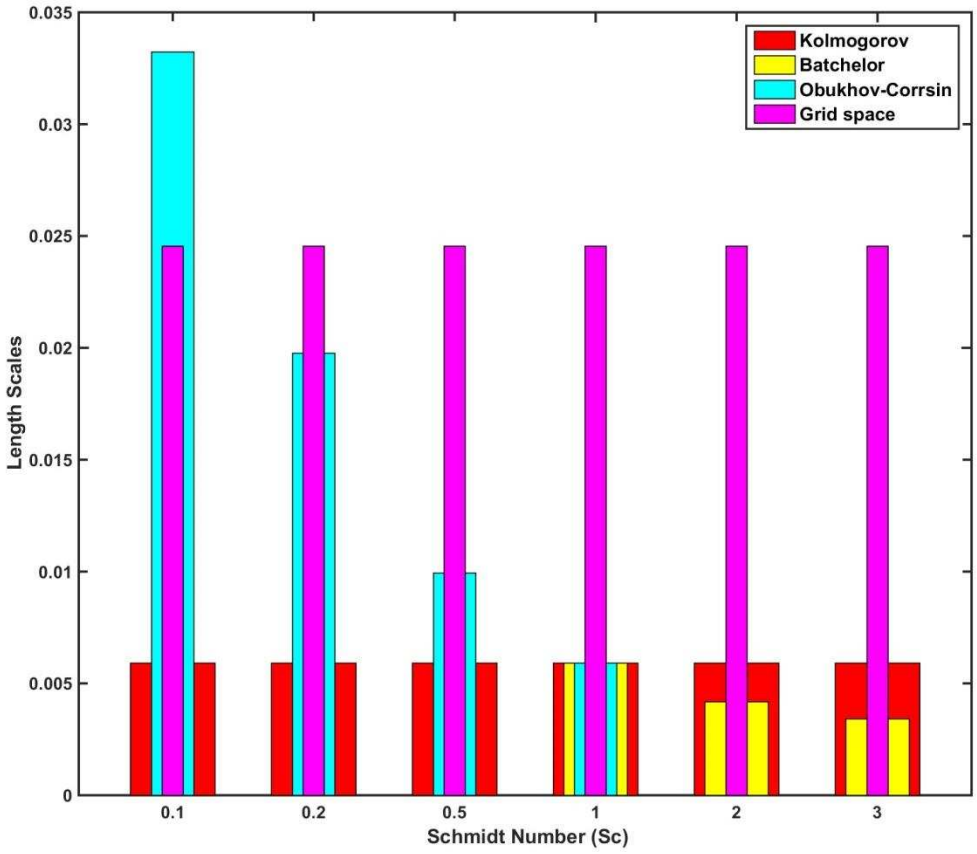

Figure 3.3: Comparison of grid scale with Kolmogorov, Batchelor and Obukhov-Corssin length scales at all Schmidt numbers for minimum wavenumber is 1.

In addition to the scale comparisons shown in Fig 3.3, another standard comparison check was done for the turbulent scalar dissipation rate ε_ρ. Given that $\varepsilon_\rho$occurs the smallest scales, it is should be expected that the simulations would not be adequately resolved to compute ε_ρ correctly. In the DNS code, turbulent statistics such as ε_ρ are computed by considering a truncated sphere within the cubic domain consisting of 256^3 grid points at each time step. It is also possible to output the scalar fluctuations ρ' on each grid point over the domain at each time separately. The

fluctuating scalar gradients of three dimensional scalar fields can then be computed at each grid points from which ε_ρ can be obtained using equation (3.6) at any given time step.

$$\varepsilon_\rho = \kappa \left\langle \frac{\partial \rho'}{\partial x_j} \frac{\partial \rho'}{\partial x_j} \right\rangle, \tag{3.6}$$

where κ is molecular diffusivity and ρ is the density of the flow. If the simulations are well resolved, both computations should yield the same results. Fig 3.4 shows the comparison for a simulation with *Sc* =1. Clearly, the results do not converge within acceptable limit. The maximum difference is more 150% and increases for *Sc* > 1.

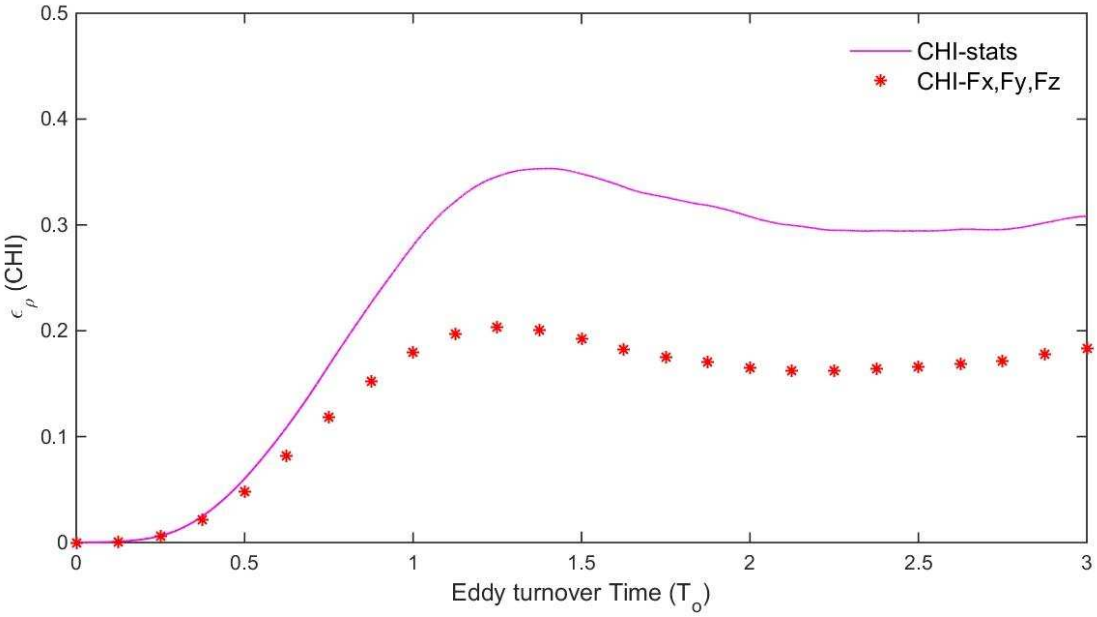

Figure 3.4: Average scalar dissipation rate $\varepsilon_\rho$computed within the DNS code and post processed ep from density fluctuations for *Sc*=1for a computational domain of length 2π.

It is clear that for a simulation with 256^3 grid points, the domain size must be smaller than 2π in order to resolve the smaller scales. Thus, the domain size was modified $\pi/2$ in order to ensure that adequate resolution of the smallest scales are obtained. The standard checks as discussed above were performed again for all *Sc* numbers and compared. As can be seen from Fig.3.5, the grid size and Kolmogorov scales are now comparable. Also the maximum difference in ε_ρ was 7%

between the results as discussed previously. Thus a box size of $\pi/2$ was used for the remainder of this study. The Schmidt number range was also restricted up to Sc=3 in order to ensure adequate resolution of Batchelor scales. The maximum difference in ε_ρ is about 17% for Sc=3 beyond which the numerical errors become large. Hence, simulations with Schmidt numbers in the range $0.1 \leq Sc < 3$ were performed with eye toward answering the overarching question related to turbulent mixing of passive scalars.

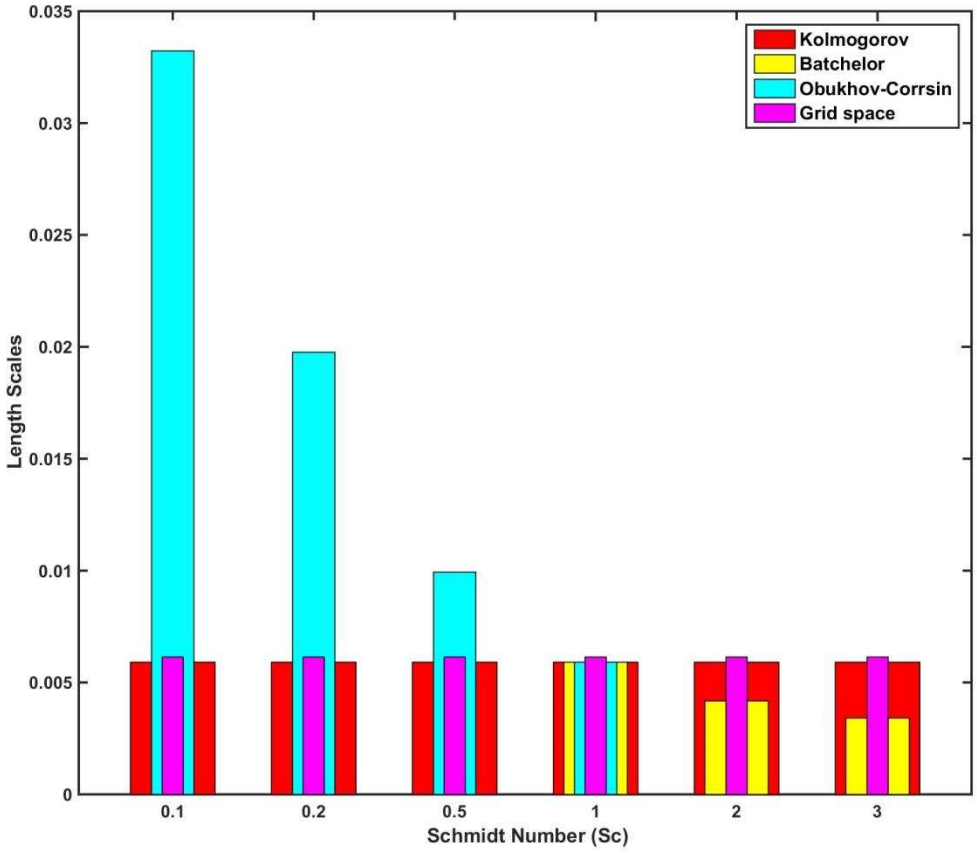

Figure 3.5: Comparison of grid scale with Kolmogorov, Batchelor and Obukhov-Corssin length scales at all Schmidt numbers for minimum wavenumber *AKMIN*=4.

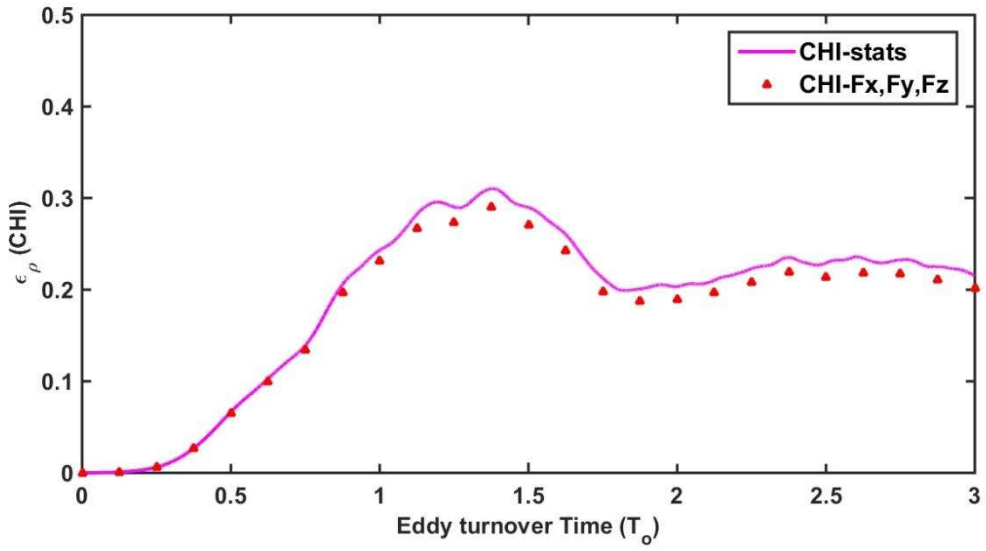

Figure 3.6: Average scalar dissipation rate ε_ρ computed within the DNS code and post processed ep from density fluctuations for *Sc*=1for a computational domain of length π/2.

3.4 Energetics

In this section, the energetics of the flow field is presented. Since all the simulations are unstratified, the energetics of the flow field does not change with varying *Sc*. Therefore, only results for *Sc*=1 simulation are discussed here.

3.4.1 Turbulent kinetic energy and dissipation rate

As a reminder, the purpose of artificially forcing the flow was to obtain a Main purpose statistically stationary velocity field for all the simulations that is turbulent. Hence, turbulent kinetic energy ($k = 1/2\langle u.u \rangle$) is constant for all time. For practical flows, the turbulent kinetic energy is produced from a sheared mean flow field. In other words, a key ingredient for the production/sustenance of turbulence is mean shear (or mean velocity gradients) in the flow. However, for homogeneous isotropic turbulence, the only way to ensure stationarity, is through artificial forcing that adds energy to the flow as discussed earlier and shown in Fig.3.1.

Available turbulent kinetic energy (TKE), turbulent potential energy and total energy are plotted in Fig.3.7 as function of time. As shown before (see Fig. 3.1) the TKE remains constant throughout the duration of the simulation.

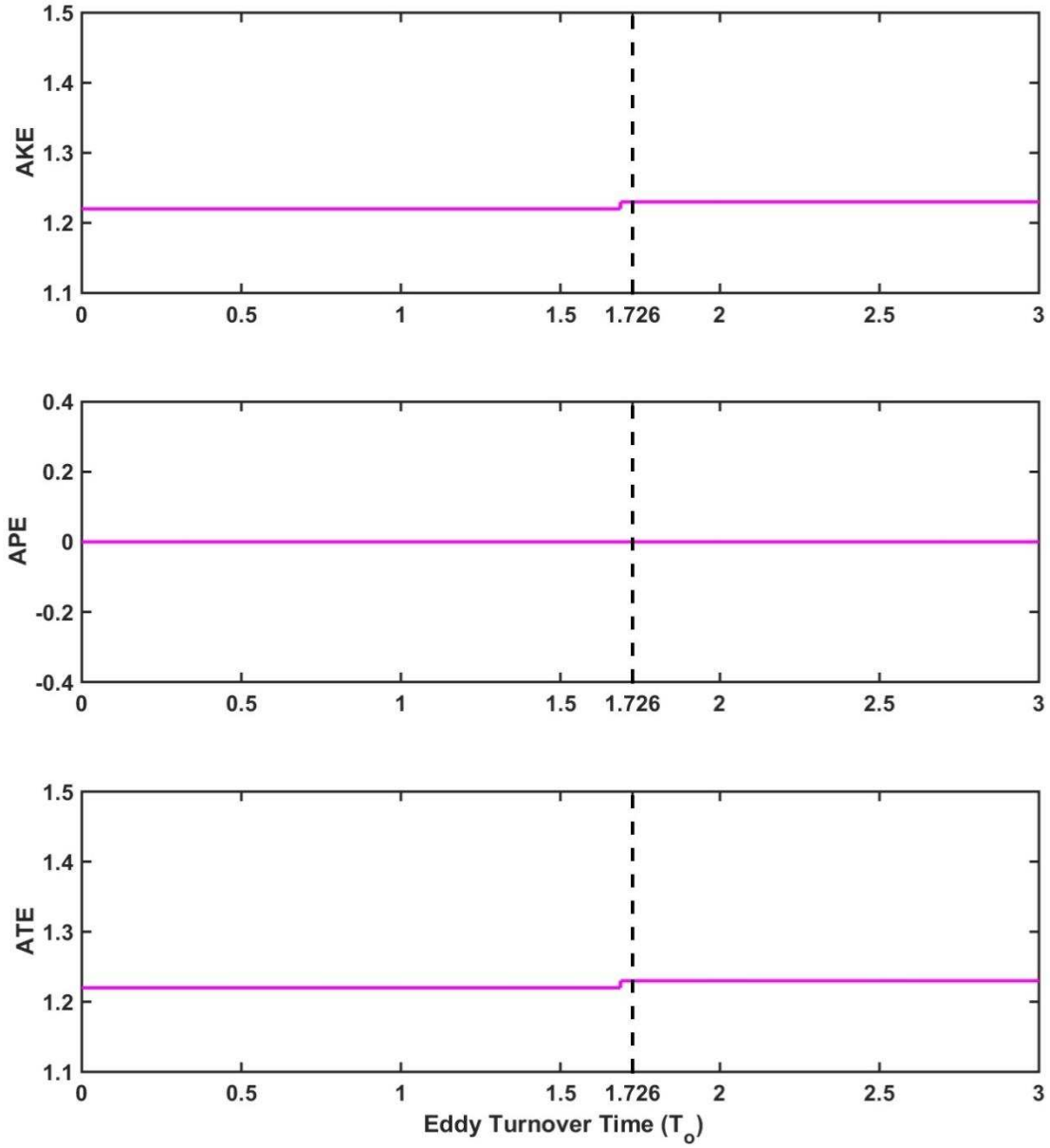

Figure 3.7: Plots of available kinetic, potential and total energies with time

It is important to note that even though the TKE is statistically stationary, this does not necessarily provide a constant rate of dissipation of turbulent kinetic energy ε_k(see Fig.3.8). ε_k is the average of square of the fluctuating velocity gradients over the domain as follow:

$$\varepsilon = \nu \left\langle \frac{\partial u_i}{\partial x_j} \frac{\partial u_i}{\partial x_j} \right\rangle, \tag{3.7}$$

where ν is the kinematic viscosity of the flow. It can be seen from Fig 3.8 that ε_k reaches its maximum dissipation at t =1.73 T_o and then it decreases slightly to attain a stationary level. Hence, the kinetic energy shows a small increment around the time of maximum dissipation (see Fig 3.7). Clearly, the potential energy is zero with no changes in time since there is no production of buoyancy fluxes for unstratified flow (Ri = 0).

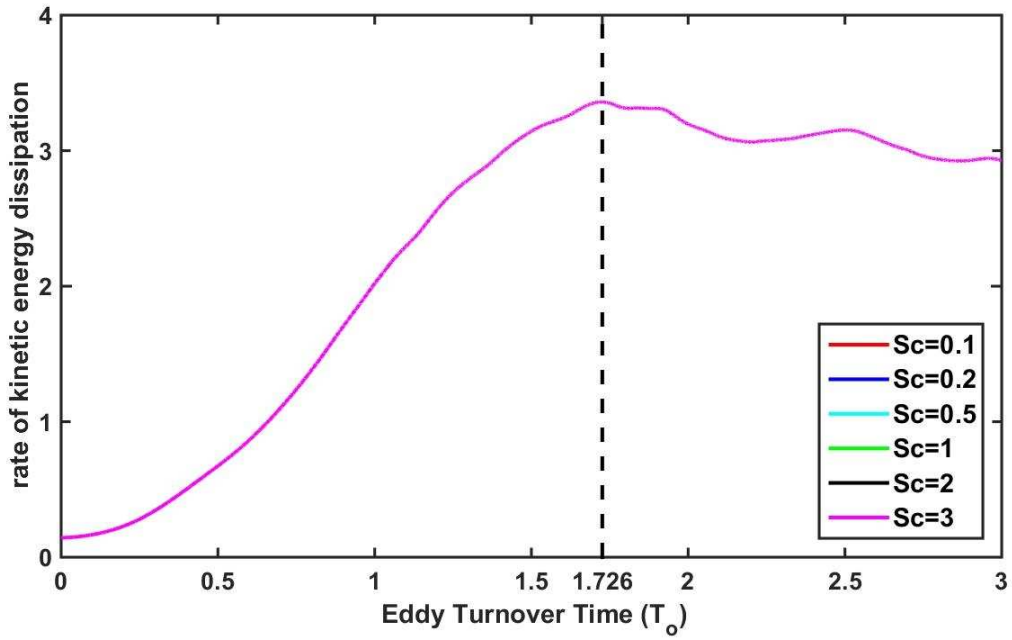

Figure 3.8: Rate of dissipation of turbulent kinetic energy ε for all Sc numbers

It can be seen from Fig 3.8 that the dissipation rate starts almost from zero and peaks at t = 1.73 eddy turnover time. During the time between t=0 to 1.73 T_o, turbulent effects start to develop

and hence it is important to use the flow statistics beyond this time for the purpose of analyzing the turbulent physics.

3.4.2 Energy and energy dissipation spectra

The energy spectrum provides the distribution of the turbulent kinetic energy as a function of wavenumber κ and is obtained as follows.

$$E_{(K)} = C_K \varepsilon^{2/3} K^{-5/3}, \tag{3.8}$$

where C_K is the Kolmogorov constant, ε is the dissipation rate of kinetic energy and K is wavenumber. Fig.3.9 shows the energy spectrum versus wavenumber at t=1.73 T_o when dissipation rate of TKE is a maximum. Here, wavenumber K ($K=2\pi/L_\eta$) is normalized by Kolmogorov length scale L_η. As discussed earlier regarding resolution issues in Sec.3.3.3, the energy spectrum reaches the Kolmogorov scales as shown by blue continuous line at high wave numbers. Hence, this is additional confirmation that the computational grid and domain resolve all scales from largest scales to smallest scales. The large scale estimate in this study is also known as the flow scale L_o where $L_o = k^{3/2}/\varepsilon_k$.

It is important to note that inertial range spectral slope in this study does not attain the classical Kolmogorov's -5/3 law (black continuous line shown in Fig. 3.9), except for a few points. This indicates that the separation of length scales are on the order of 1 to 10 for these simulations at an initial Reynolds number Re_o=625. The Taylor microscale Reynolds number Re_λ~200. The Reynolds number should be sufficiently high enough to achieve a considerable order of separation of scales. It has been found that a minimum Taylor Reynolds number of about Re_λ~2000 is needed to achieve -5/3 slope (Sreenivasan 1995).

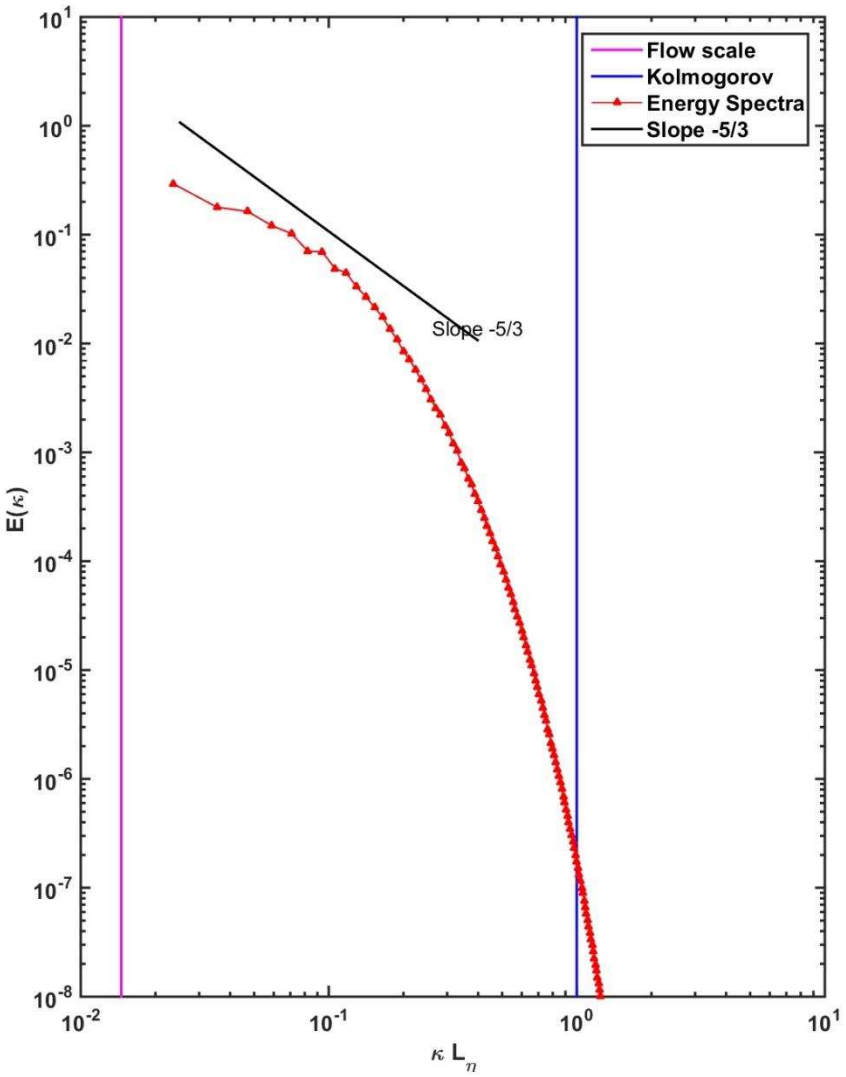

Figure 3.9: Energy spectrum with wavenumber normalized by Kolmogorov length scale for *Sc*=0.1 and *Sc*=1 at maximum energy dissipation. Black line indicates the Kolmogorov law of -5/3 slope at inertial subrange.

Fig.3.10 shows the energy dissipation spectra at different times for *Sc*=1. These plots clearly indicate peaks in energy dissipation at low wavenumbers and subsequent decay at middle wave numbers that approaches zero at high wavenumbers. The spectra at different times are exhibiting the same trend with the spectrum at *t*= 1.73 eddy turnover time indicating maximum dissipation. The monotonic and decaying trend in the dissipation spectra is another diagnostic that indicates that the simulations are well resolved with no contamination or aliasing errors occurring at higher wavenumbers (i.e. smaller scales).

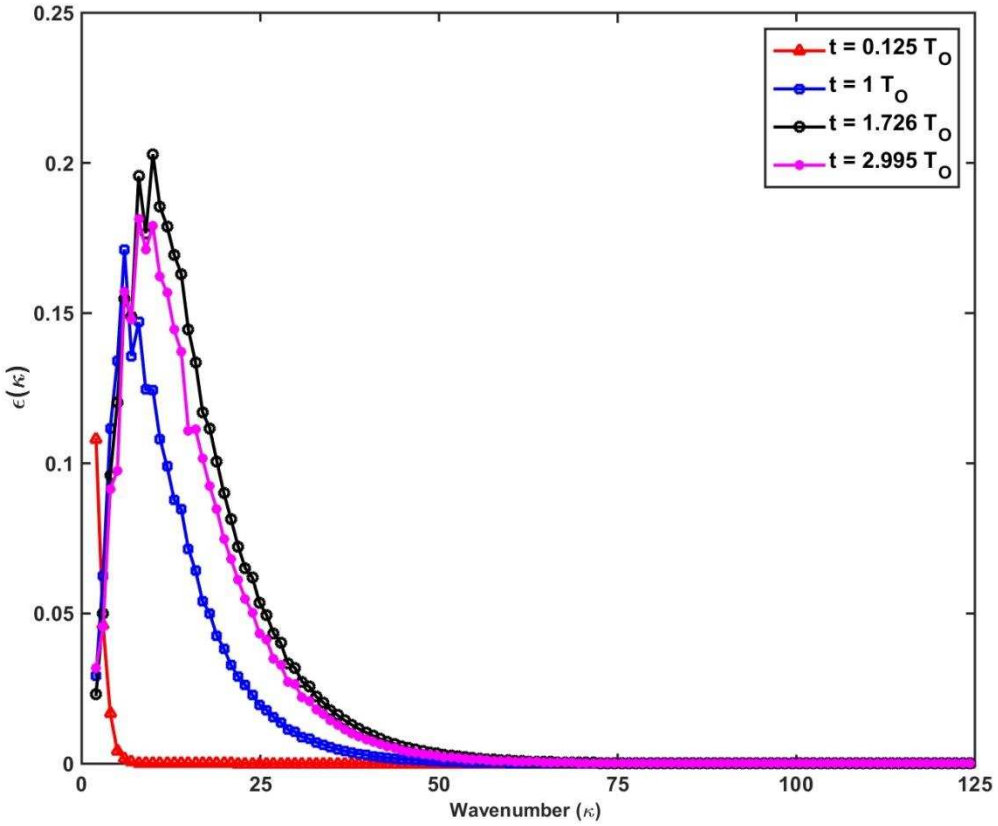

Figure 3.10: Energy dissipation spectra with wavenumber κ of Sc=1 at different time steps when t = 0.125 T_O, 1 T_O, 1.726 T_O & 2.995 T_O.

3.5 Scalar and scalar dissipation rate

Since the simulations presented in this chapter were conducted for unstratified flow (Ri = 0), the density acts as a passive scalar, and hence it does not influence the dynamics of the flow via buoyancy effects. Here, the density field is therefore used as a passive scalar. Also, it should be noted that the Schmidt numbers ($Sc = \frac{\nu}{\kappa}$) will influence the scalar properties. Note for Sc<1, the molecular diffusivity of the scalar is greater than momentum diffusivity and vice versa for Sc>1.

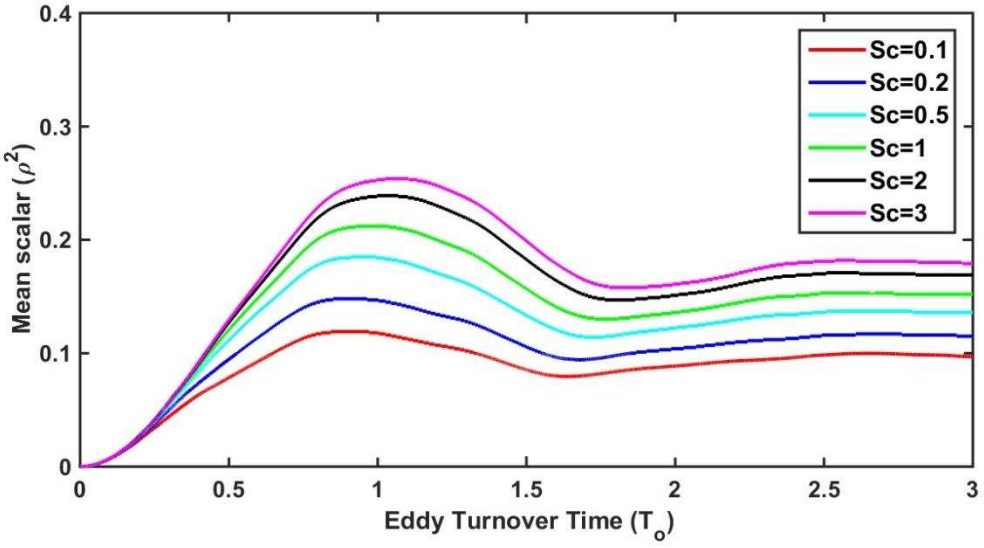

Figure 3.11: mean square of scalar (density) fluctuation is plotted with time for *Sc*= 0.1, 0.2, 0.5, 1, 2 & 3.

The mean square of density (scalar) fluctuations ($< \rho'^2 >$) (also known as the scalar variance) is plotted with eddy turn over time for all Schmidt numbers in figure 3.11. The mean square scalar (density) fluctuations increases from zero and reach their peaks after about the first eddy turn over time and then decrease to almost quasi-steady state further in time. It can be seen that the trends for all Schmidt numbers are the same with higher fluctuations with increasing *Sc*. A similar behavior is observed for scalar dissipation rates $\left(\varepsilon_\rho = \nu \left\langle \frac{\partial \rho'_i}{\partial x_j} \frac{\partial \rho'_i}{\partial x_j} \right\rangle\right)$ which are shown in Fig.3.12. Once stationarity is achieved (after about one turn over time), the scalar properties continue to be influenced by the Schmidt number. For *Sc*< 1, it can be seen at least for Reynolds numbers of these simulations that the scalar variance and they are smaller compared their counterparts at *Sc*>1 but the scalar dissipation rates appear to converge at later times for all *Sc*.

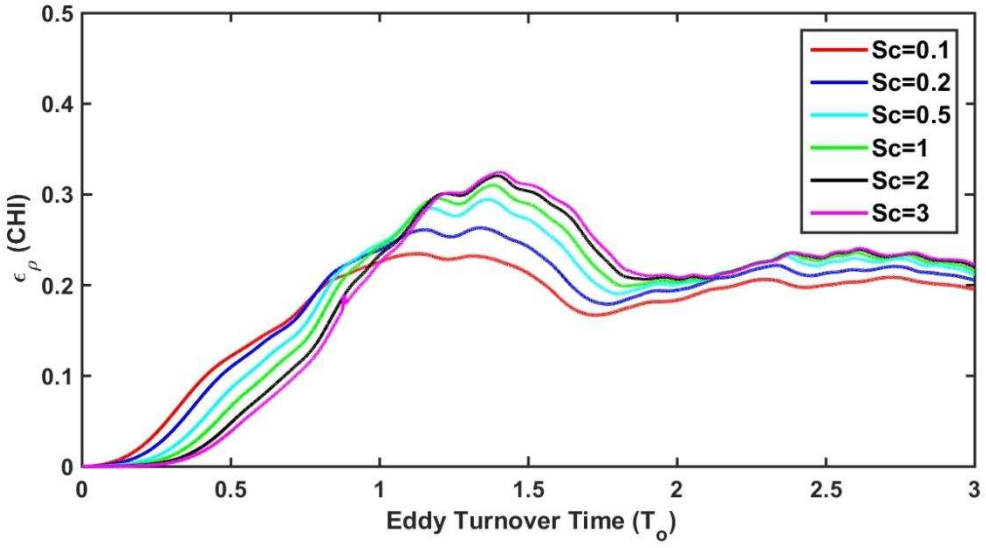

Figure 3.12: variation of scalar dissipation (CHI) with time for *Sc*= 0.1, 0.2, 0.5, 1, 2 & 3.

In order to assess whether the turbulent scalar diffusion is the predominant process (as opposed to molecular diffusion) in these simulations, the ratio between the turbulent diffusivity K_S, and molecular diffusivity κ, was computed. This ratio is known as non-dimensional diascalar diffusivity or commonly known in oceanography as the Cox number (C_X) given by Eq. (3.9). Fig.3.13 shows the non-dimensional diascalar diffusivity as a function of time for all *Sc*.

$$C_X = \frac{K_S}{\kappa}, \tag{3.9}$$

Note the diascalar diffusivity K_S is defined as

$$K_S = \frac{\epsilon_\rho}{\left(\partial \overline{\rho}'/\partial z\right)^2}, \tag{3.10}$$

The results for the non-dimensional diascalar diffusivity for all Schmidt numbers clearly show that turbulent diffusion dominates. For *Sc* = 0.1, $K_S/\kappa = 15$ and reaches up to 400 at steady state for *Sc* =3. Thus, these results confirm that the scalar mixing in these simulations are driven by the turbulence.

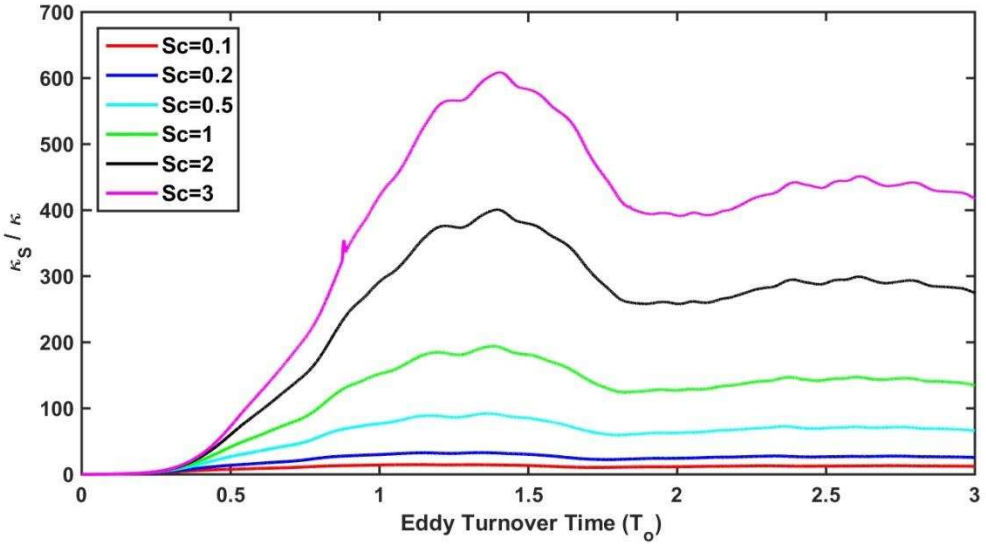

Figure 3.13: Non-dimensional diascalar diffusivity plotted with time for all Schmidt numbers.

Statistical geometry of isovalues of scalar dissipation rates are shown in Fig.3.14 for selected *xz* planes where y=128. The distributions are shown for *Sc*=0.1 and 1 at different times. The ramp and cliffs structures seen in the distributions indicate regions of sharp changes in scalar dissipation rate ε_ρ. At initial time t= 0.5 T_o, the scalar dissipation rates exhibit very low values that are fairly uniform over the xz plane except for a very few sharp changes in the middle of plane for both Schmidt numbers. Peaks in the scalar dissipation occurs at t=1.75 T_o and higher fluctuations of scalar dissipation are widely spread over the plane at t= 1.75 T_o and 3 T_o for both Schmidt numbers. However, higher amplitudes are seen for *Sc*=1 compared to *Sc*=0.1 (as also indicated previously in Fig.3.12).

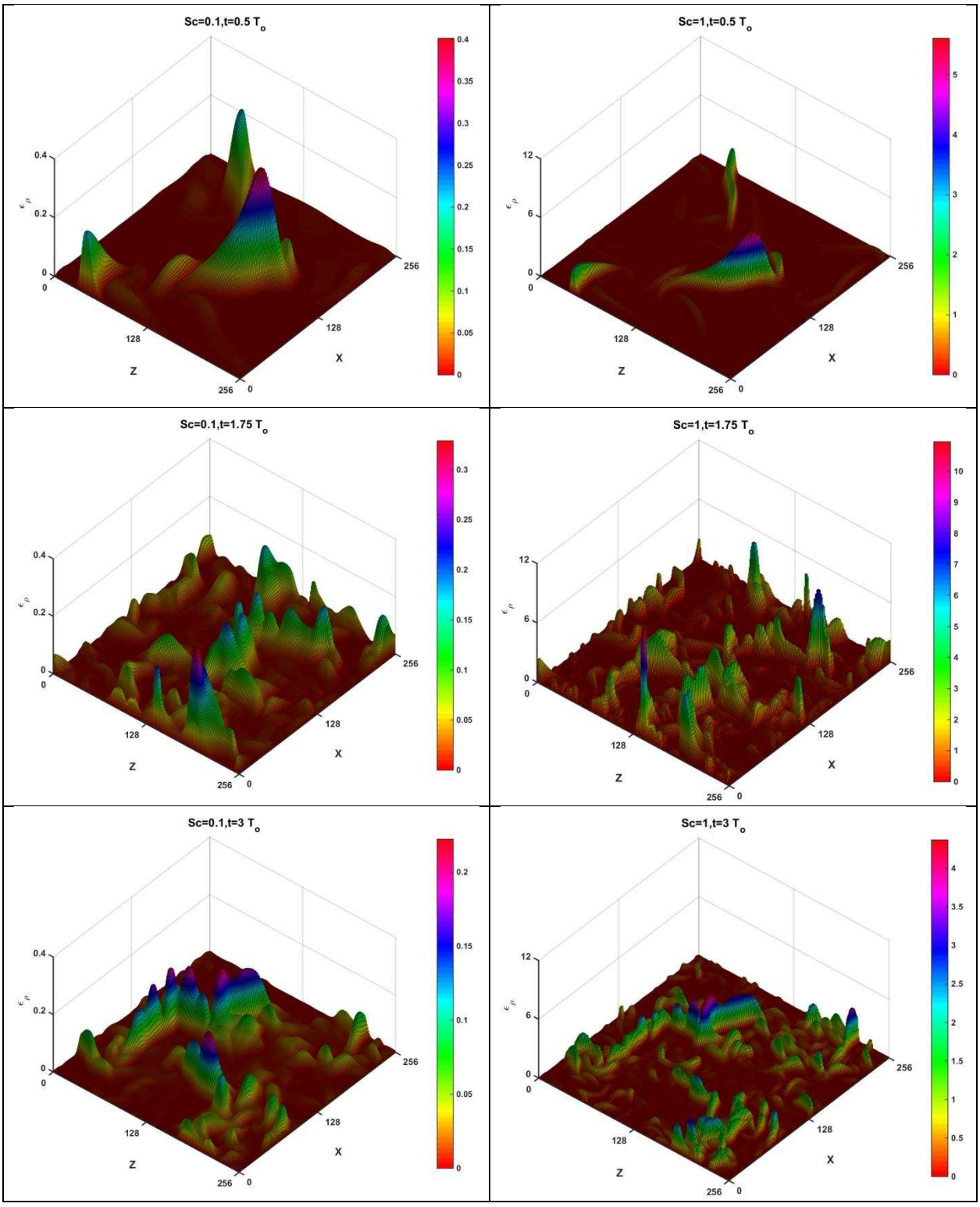

Figure 3.14: Contour surfaces of scalar dissipation (CHI) amplitudes at different times for *Sc*= 0.1 and 1 are plotted for selected plane at *y*=128.

3.5.1 Scalar and Scalar dissipation spectrum

For scalars, the form of the spectrum $E_{\rho(\kappa)}$ whose integral gives the scalar variance, is sensitively dependent on how the smallest scales compare with the smallest momentum scales. Multiple regimes are formed depending on the Schmidt numbers as described previously in Fig. 2.1 in Chapter 2 (Gotoh and Yeung, 2012). Fig.3.15 shows the scalar spectra for different Schmidt numbers. In Fig.3.15 (a), slopes of -1 and -17/3 are indicated to show the trend of inertial-diffusive range and viscous-convective range, respectively.

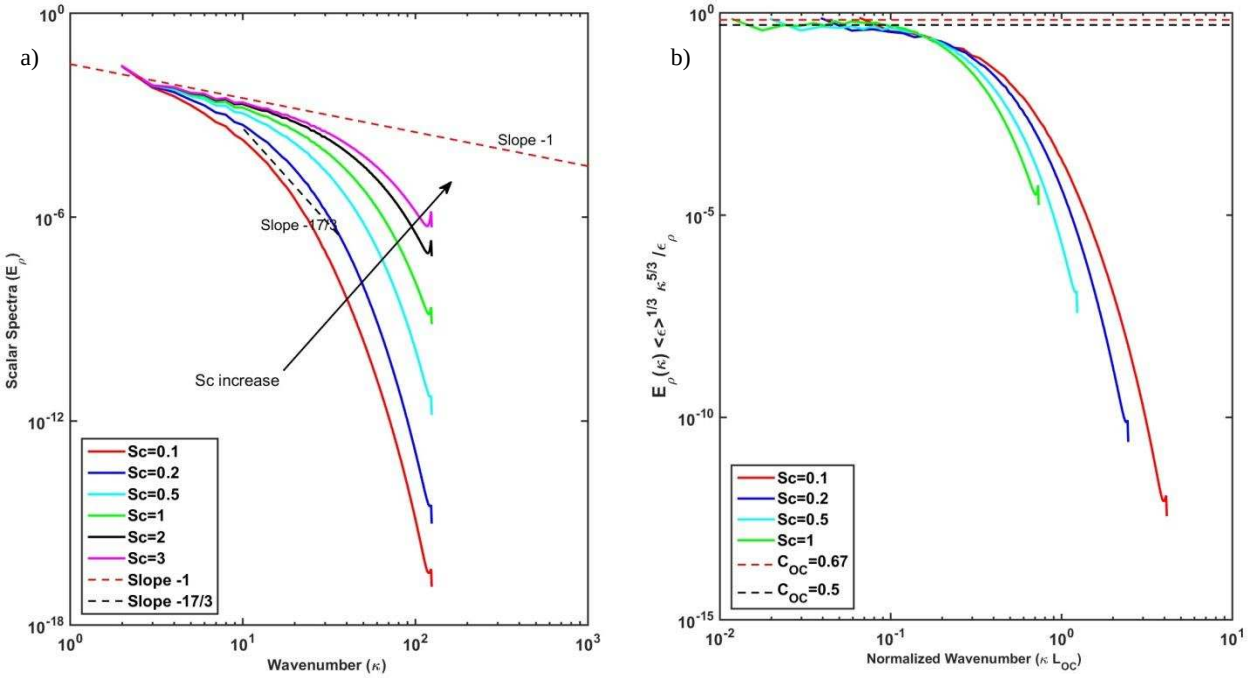

Figure 3.15: a) Scalar spectra plotted with wavenumber for all *Sc* numbers and slopes of -1 and -17/3 are shown in viscous-convective and inertial-diffusive regimes respectively. b) Scalar spectrums for low *Sc* numbers $Sc \leq 1$ in Obukhov-Corrsin scaling is plotted with wavenumber normalized by L_{OC}.

For low Schmidt numbers $Sc \leq 1$, a small range of the scalar spectrum reaches the slope of -17/3. However, most of the spectra do not capture this limit perhaps due to the low Reynolds number of the simulations. When *Sc* increases (as indicated by the black arrow in Fig 3.15(a)), scalar spectrum also increases towards the slope of -1, which indicates the region of viscous-

convective regime (that must hold for Sc >1). Again, due to the low Reynolds numbers of the simulations, the turbulent scale separation was not sufficient to reach the expected trends as shown in Fig.2.1.

The scalar spectra are scaled with Obukhov-Corrsin length scale L_{OC} and plotted in Fig.3.15 (b) for low Schmidt numbers $Sc \leq 1$. All spectra in the low wavenumber band start from a near constant level which is known as the Obukhov-Corrsin constant C_{OC} which is about 0.5 in this set of simulations. The asymptotic value is $C_{OC} = 0.67$ as suggested by Sreenivasan (1996) for $Re_\lambda > 1000$.

3.6 Coherent turbulent structures

A turbulent flow can be considered as a stochastic vortical flow. Coherent structures can be considered as signatures of vertical motions in the flow. These structures can be identified by flow visualization or by other eduction techniques from the DNS data. However, they are very difficult to define and distinguished precisely for the purpose of quantitative description of the turbulent motions. The coherent structures are generally significantly larger than the smallest turbulent scales. The purpose here is to illustrate such structures in the simulations done in this study and provide a perspective on how they evolve spatially and temporally. Isosurfaces are selected based thresholds in order to provide a good qualitative description of the structures.

3.6.1 Enstrophy and Vorticity

Since turbulent eddies are generally characterized by vortical motions, it is insightful to visualize the vorticity fields. Both the horizontal vorticity and the vertical vorticity fields are visualized. The mean square vorticity known as the enstrophy is also utilized for describing the flow structures.

The isosurfaces of enstrophy, horizontal and vertical vorticity for the simulation with Sc=1 are plotted in Fig.3.16 at different times. Just after the initialization at t=0.125 T_O, there is very little vortical motion as can be seen from all three diagnostics. As time progresses, the flow evolves considerably with tube-like patches developing significantly. The structures fill the whole domain and the classic tube-like structures seen in other similar DNS studies of homogeneous isotropic turbulence are observed.

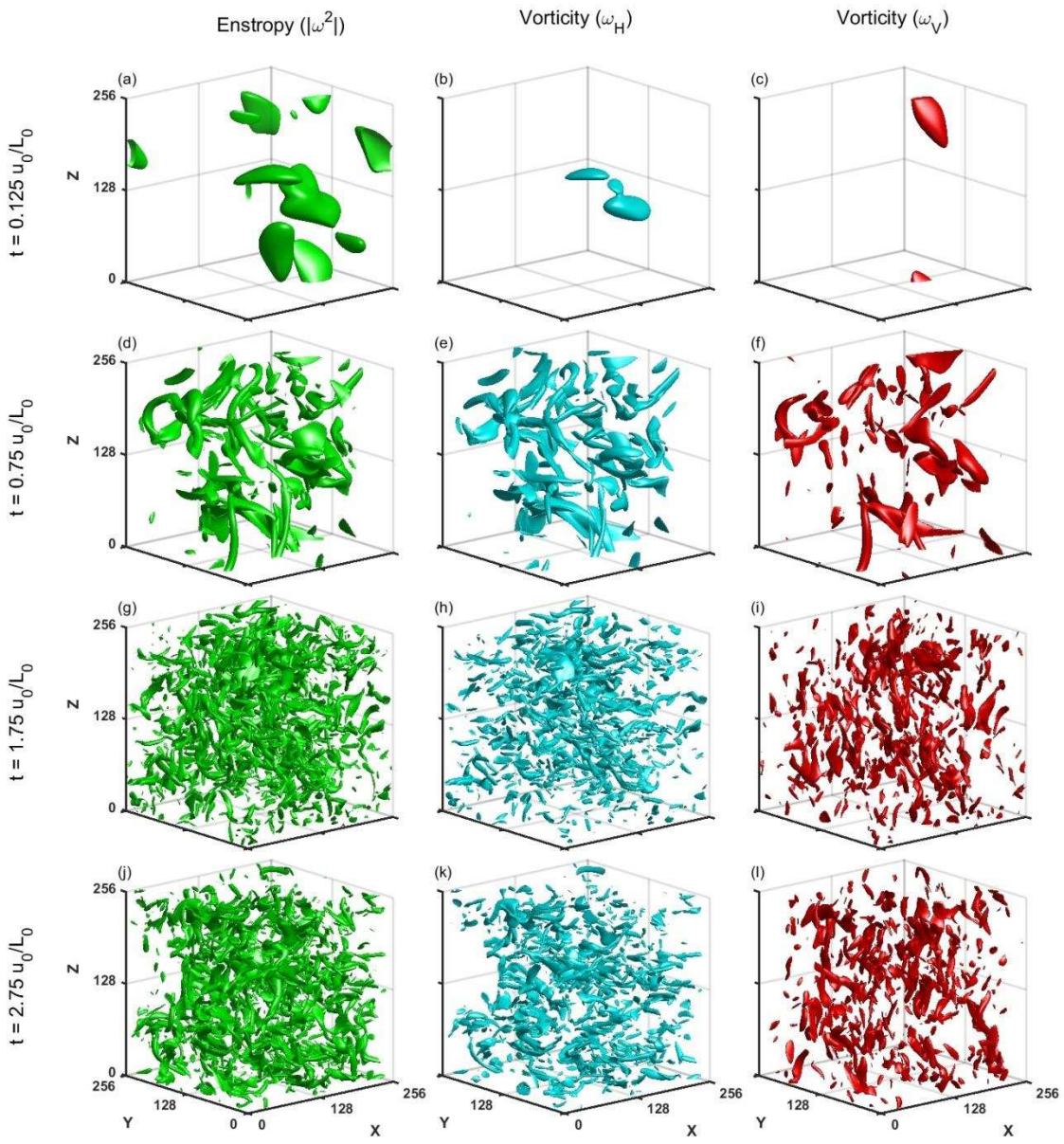

Figure 3.16: Isotropic structures of enstrophy, horizontal vorticity and vertical vorticity for *Sc*=1 at different time steps. Selected threshold of 2.5 times the root mean square (rms) of enstrophy

3.6.2 Scalar and scalar dissipation

Fig.3.17 through 3.20 show the scalar fluctuations and scalar dissipation fields for Schmidt numbers 0.1, 1, and 3, respectively. At time t= 0.125 T_o, scalar fluctuations and scalar dissipation patches follow a similar pattern for all *Sc* numbers. As time progresses, the patches evolve into more turbulent like features. What is most obvious is the patches for the higher Sc simulations are clearly more turbulent which is in agreement with the higher quantitative values of the diascalar diffusivity presented in Fig. 3.13.

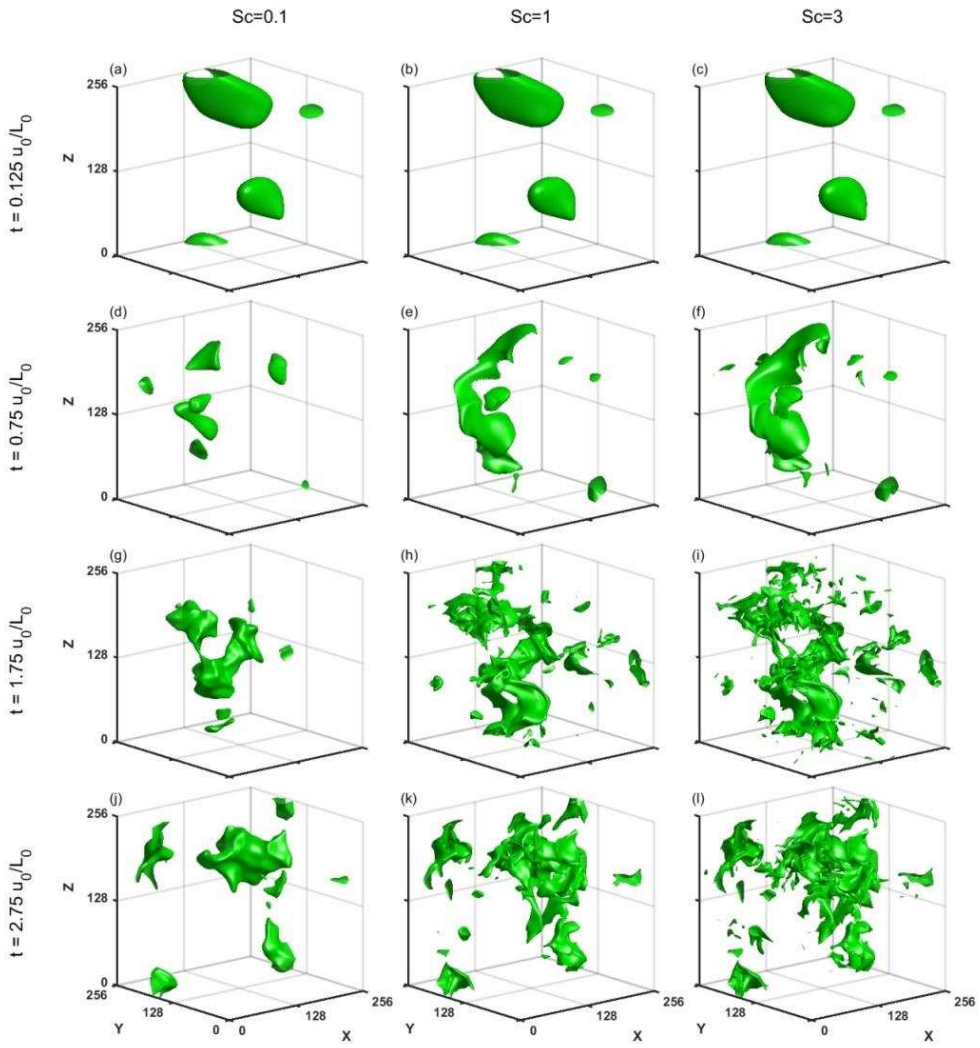

Figure 3.17: Isosurfaces of scalar (density) fluctuations for *Sc*=0.1, 1 & 3 at different time steps. Isosurfaces are mapped with selected threshold of 2 times the root mean square (rms) of scalar fluctuation.

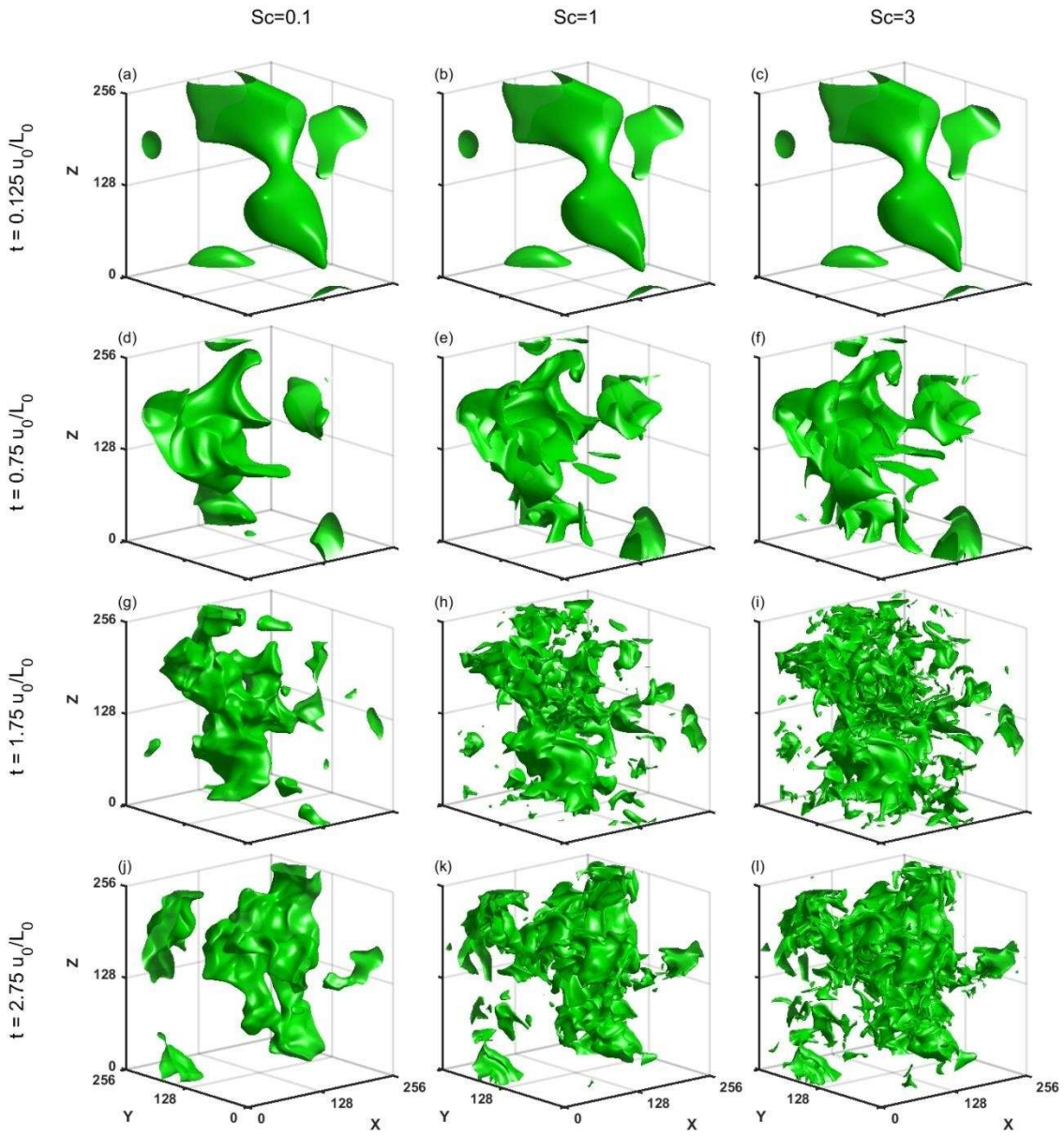

Figure 3.18: Isosurfaces of scalar (density) fluctuations for *Sc*=0.1, 1 & 3 at different time steps. Isosurfaces are mapped with selected threshold of 1.5 times the root mean square (rms) of scalar fluctuation.

Note, Fig.3.17 is patched for 2 times the rms of mean scalar fluctuations and Fig.3.18 is mapped with a threshold of 1.5 times rms of mean scalar fluctuations. Also, the scalar dissipation rates are plotted with two different thresholds in Fig.3.19 and 3.20, respectively. Scalar dissipation in these plots also follows a same trend like as scalar fluctuation isosurfaces in Fig.3.17 and 3.18.

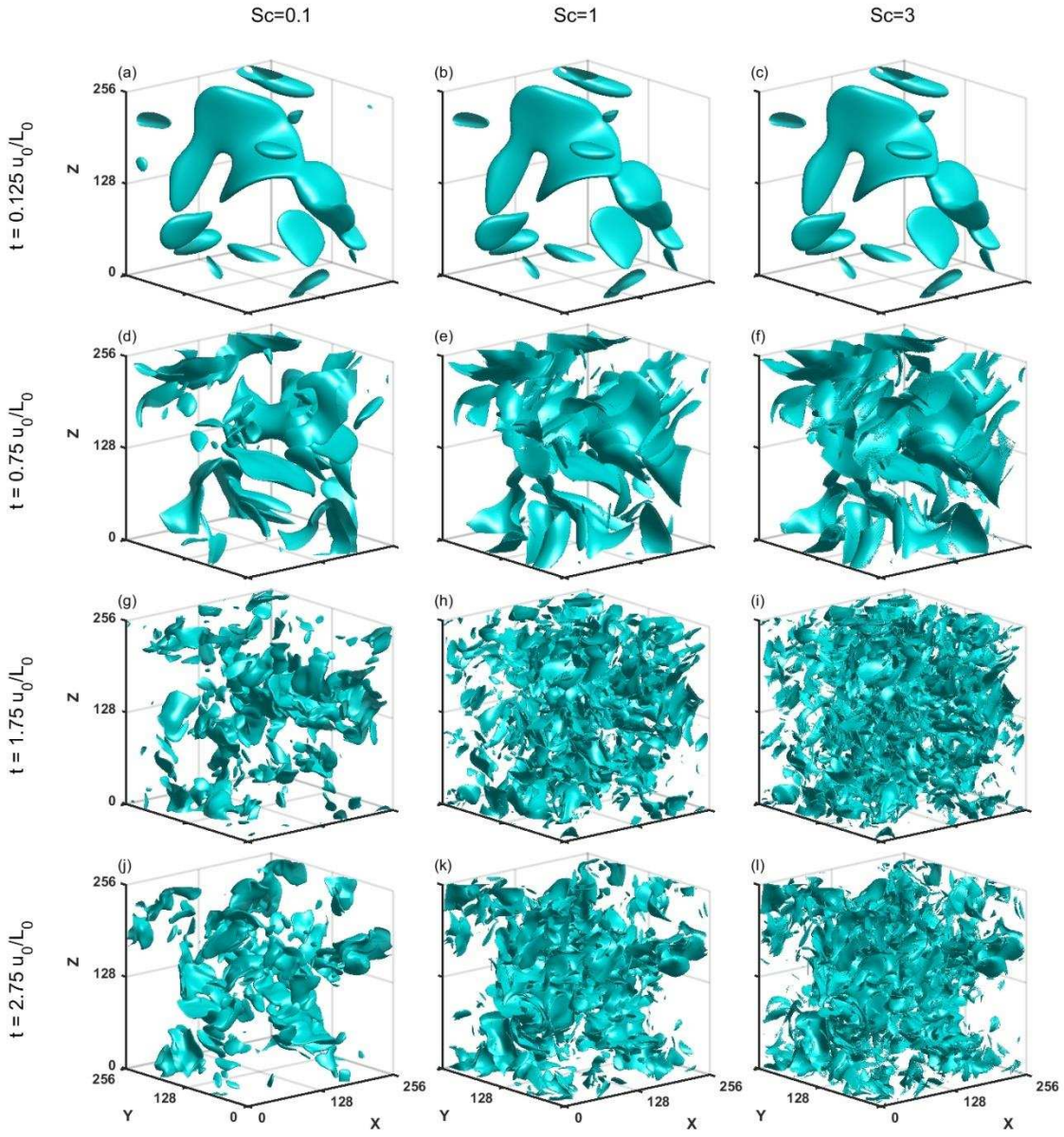

Figure 3.19: Isosurfaces scalar dissipation rate for *Sc*=0.1, 1 & 3 at different time steps. Isosurfaces are mapped with selected threshold of 2 times the root mean square (rms) of scalar dissipation.

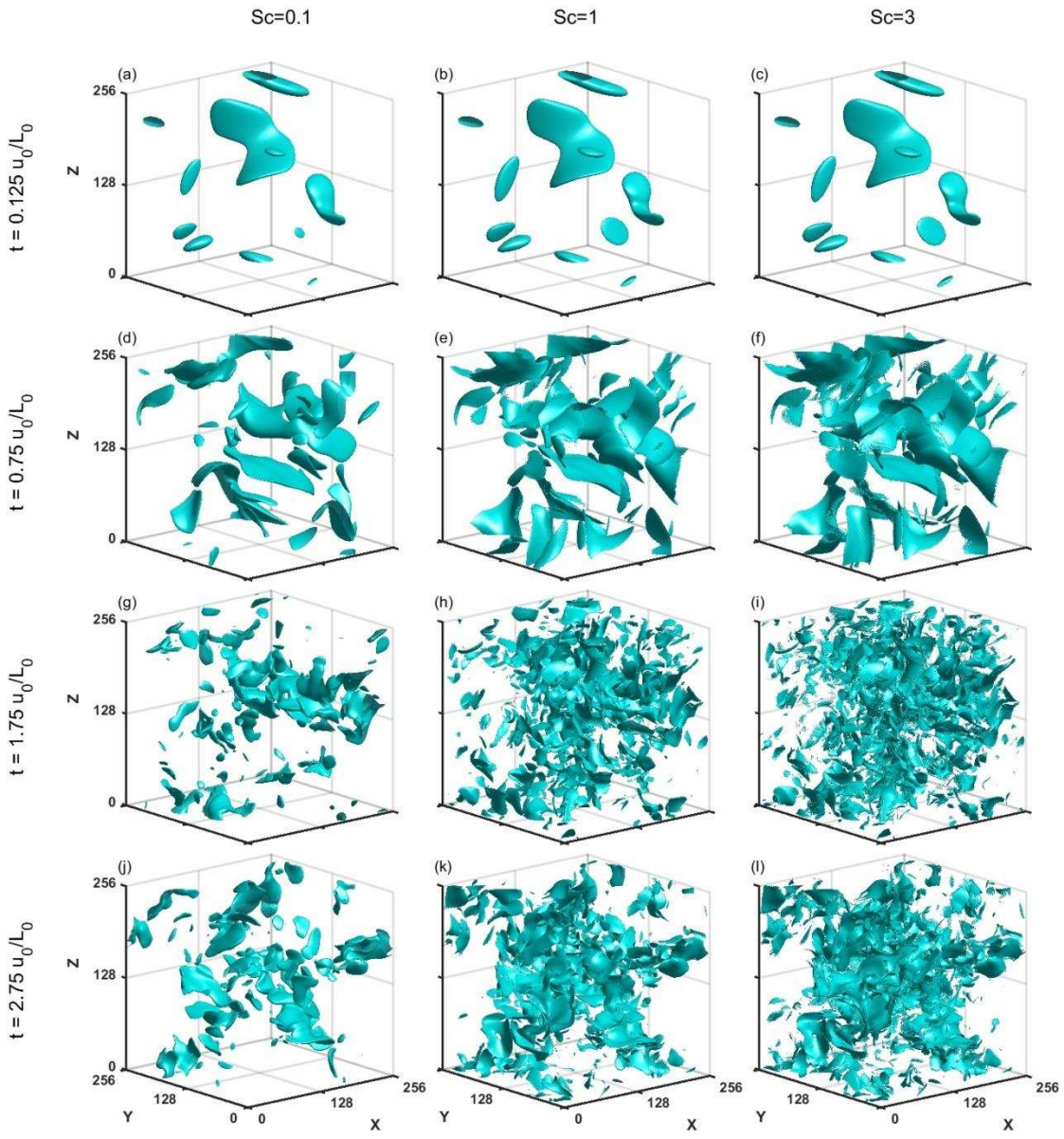

Figure 3.20: Isosurfaces scalar (density) dissipation rate for *Sc*=0.1, 1 & 3 at different time steps. Isosurfaces are mapped with selected threshold of 3 times the root mean square (rms) of scalar dissipation.

3.7 Modeling for turbulent scalar mixing

The ability to quantitatively model/predict the turbulent mixing of passive scalars is important in many engineering and geophysical applications. The major challenge from a practical standpoint is to determine the key large scale turbulent parameters that must be measured in the field or modeled in numerical simulations in order to predict the turbulent mixing which occurs at the small scales. In other words, what are key ingredients required for predicting the turbulent diascalar diffusivity K_S? Furthermore, the quantities that are considered should be fairly straightforward and inexpensive to measure in the field such as in oceanic flows or for simulations, such quantities should be obtained without extreme computational costs. With these constraints in mind, the ambitious goal in this section is to develop a simple but robust model for the diascalar diffusivity that can used in field applications as well as a turbulence closure model in computational simulations of fluid flows involving passive scalars.

The model proposed by Venayagamoorthy and Stretch (2006, hereafter the VS model) for the turbulent diascalar diffusivity is used as a basis to develop a practical model. The VS model is given as:

$$K_S = \gamma' \frac{{L_E}^2}{T_L}, \tag{3.11}$$

where, $L_E = \overline{\left(\rho'^2\right)}^{1/2} / |\partial\rho'/\partial z|$ is the Ellison 'overturning' length scale, $T_L = k/\varepsilon$ is turbulent time scale and γ' is one-half of the mechanical to scalar time scale ratio.

In a follow-up work, Stretch and Venayagamoorthy (2010) showed that VS model was quite robust for predicting the diascalar diffusivity using datasets from numerous laboratory and DNS studies that were done by different researchers. However, the VS model is not quite practical for field scale applications in that, it does not require the prescription of the turbulent time

scale $T_L = k/\varepsilon$. It is clear that this quantity would be very challenging to estimate or quantify a priori given that ε is a small-scale turbulent quantity. Therefore, the goal here is to obtain a simplification to the VS model that only relies on large scale (measurable) quantities to estimate K_S.

As a first check, the non-dimensional diascalar diffusivity (K_S/κ) computed from the six different simulations performed in this study for passive scalars in an unstratified flow are compared in Fig.3.21 against the predictions of the VS model. It is clear that the actual values from the DNS simulations are closely predicted by VS model with some small variations. The results confirm that the VS model can be extended to passive scalars without any loss of generality (noting that Stretch and Venayagamoorthy 2010 already showed that VS model can be extended to passive scalars). Note that Fig.3.21 is a non-dimensional plot of-diascalar diffusivity (K_S/κ) or Cox number, versus the turbulent Peclet number ($Pe_t = {L_E}^2/T_L\kappa$), where κ is the molecular diffusivity ($\kappa = \nu/Sc$).

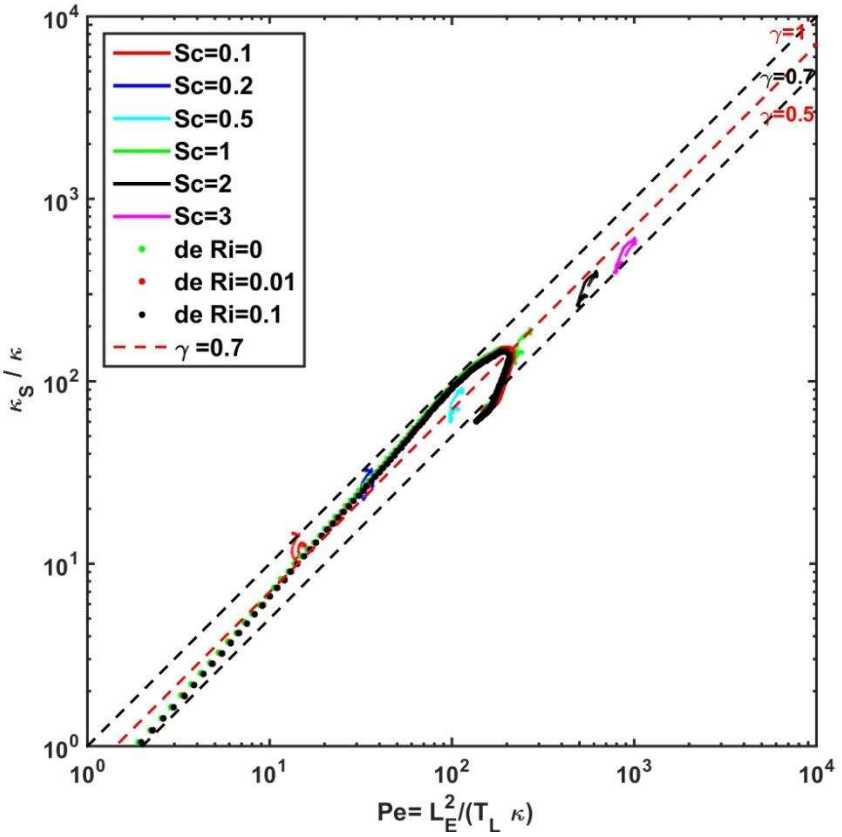

Figure 3.21: Non-dimensional diascalar diffusivity for different Schmidt numbers with turbulent Peclet number. Dashed black lines represents γ'=1 and 0.5.

For further confirmation of the γ' value of 0.7 proposed by VS, DNS results from decaying unstratified turbulent flows with a passive scalar were added to the current results. γ' was computed from the mechanical-to-scalar time scale as shown in Eq. (3.12).

$$\gamma' = \frac{1}{2}\frac{\varepsilon_\rho T_L}{\overline{(\rho'^2)}/2}, \tag{3.12}$$

where, ε_ρ scalar dissipation, T_L is the turbulent time scale ($T_L = k/\varepsilon$) and ρ' is mean scalar. Fig.3.22 shows γ' as function of time from which it can be seen that a value of 0.7 is a good estimate for the average value of γ' once the flow has reached stationary conditions, consistent with the estimate proposed in VS model.

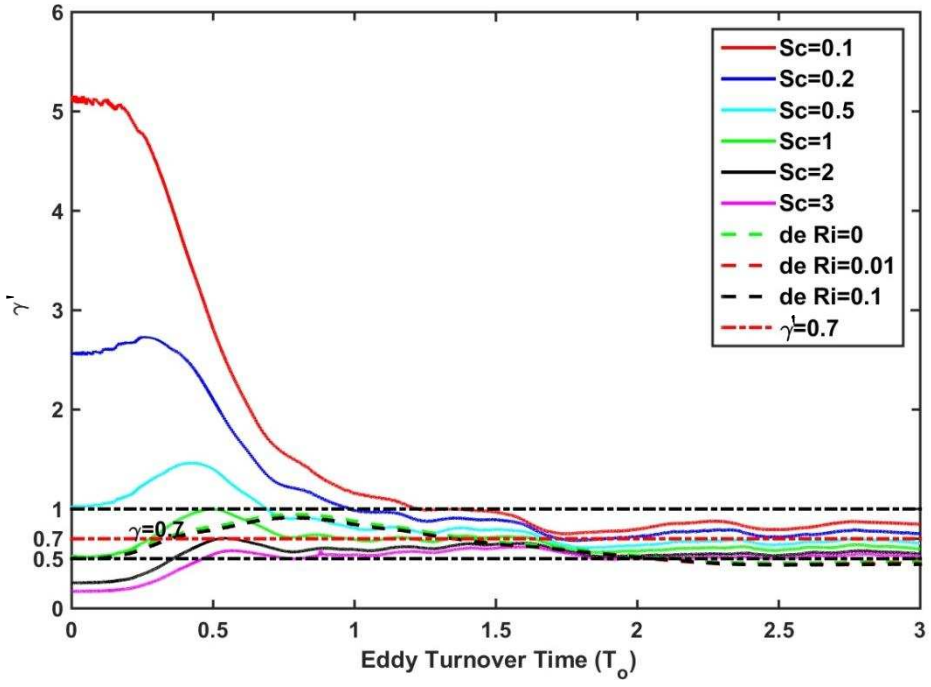

Figure 3.22: Gamma values for passive scalars for different Schmidt numbers in forced and decaying flows.

Now, to improve the VS model for practical application (as alluded earlier to), the need for an easily measurable mixing length scale that mimics the Ellison length scale L_E is required. Furthermore, a further recasting of the VS model is required in order to circumvent the need to prescribe the time scale T_L. From the stably stratified turbulence literature (especially related to oceanic flows), a strong linear (almost one to one) correlation between the Ellison length scale and the Thorpe length scale L_T has been established (Itsweire et al. 1993, Mater et al., 2013). The natural question that follows is whether a similar relationship would be valid for passive scalars in unstratified flows? Of course, it must be noted that Thorpe length scales in unstratified flows can no longer be related with the available potential energy in the flow. Regardless, it should still be a representative indicator of the mixing length scale. L_T can be calculated from the scalar fluctuating field by resorting the distribution monotonically. The detailed procedure is well described in Mater et al. (2013). The L_T were computed for all the six different DNS runs at different times and

compared with L_E as shown figure 3.23. It can be seen that there is a remarkably good agreement between L_E and L_T. In fact, it is found that $L_T = 0.8\ L_E$, a relationship first suggested Itsweire et al. (1993) for stably stratified shear flows as shown in Fig.2.2. This study shows that this relationship also holds for passive scalars in unstratified flows and hence suggests that L_E can be replaced with $L_T/0.8$.

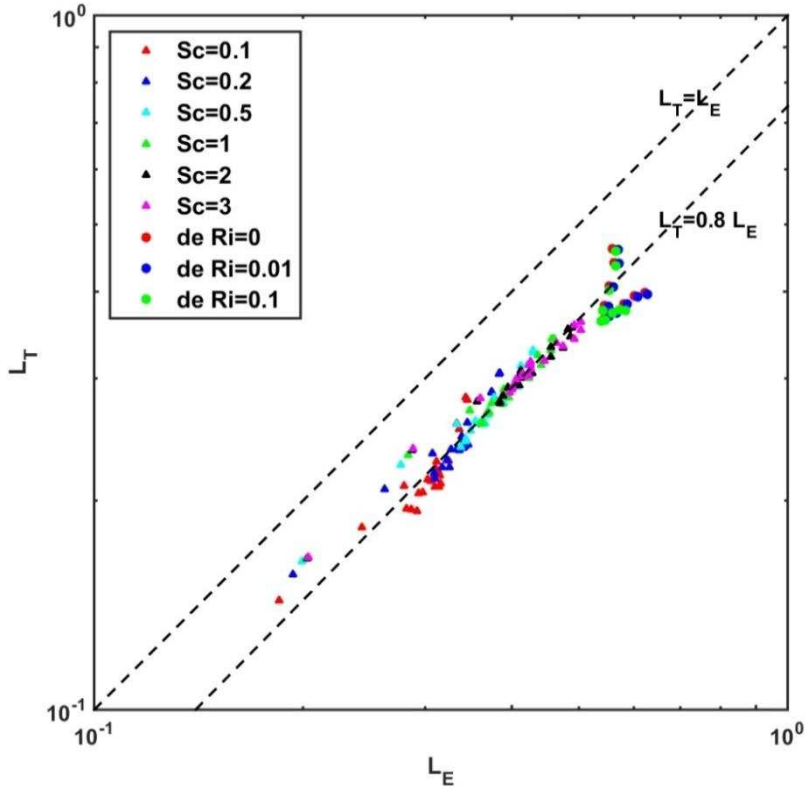

Figure 3.23: Thorpe scalar length versus Ellison length scale for Passive scalars.

The next issue is to find a suitable alternative formulation for the turbulent time scale $T_L = k/\varepsilon$. Using dimensional reasoning T_L can be rewritten in terms of the widely known turbulent kinetic energy length scale $L_{k\varepsilon}$, as $T_L = k^{3/2}/\varepsilon k^{1/2} = L_{k\varepsilon}/k^{1/2}$, where k here is the turbulent kinetic energy (Pope 2000). Hence, turbulent time scale can be recast in terms of a turbulent length scale $L_{k\varepsilon}$ and a velocity scale given by $k^{1/2}$. Intuitively, it is plausible that the turbulent length scale $L_{k\varepsilon}$ should also correlate linearly with L_E. Figure 3.24 shows a plot of $L_E/L_{k\varepsilon}$ versus time

once the flow has reached a quasi-steady state while Fig 3.25 shows a plot of L_E versus $L_{k\varepsilon}$. As can be seen, there is almost one to one correspondence between these two length scales with an average relationship given by $L_E = 0.9L_{k\varepsilon}$.

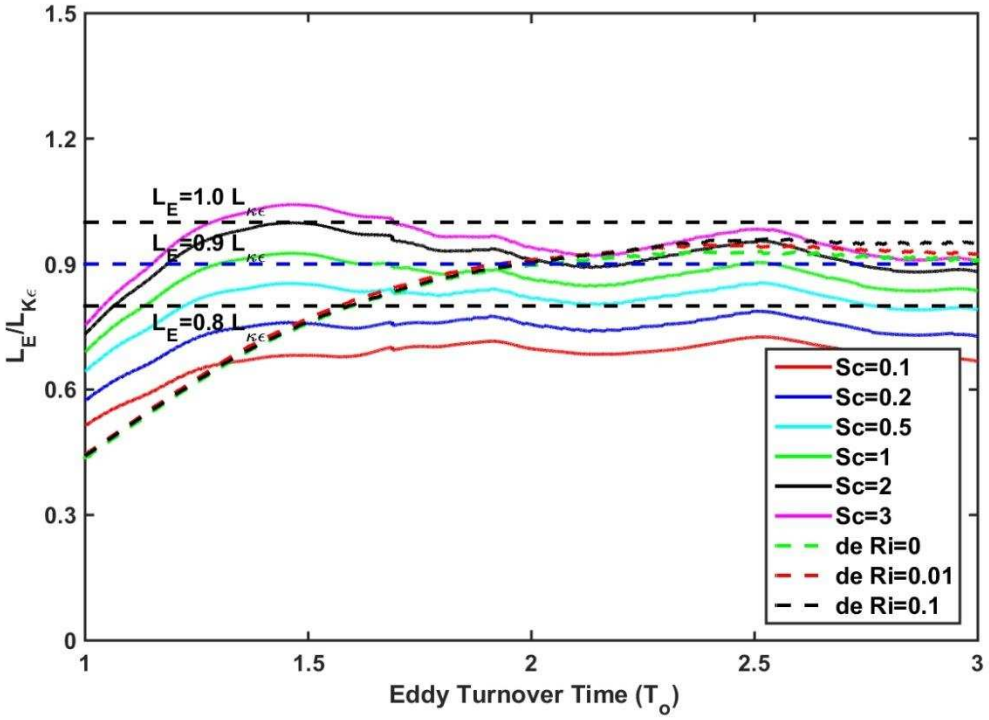

Figure 3.24: Ratio of $L_E/L_{k\varepsilon}$ with time after the flow has developed.

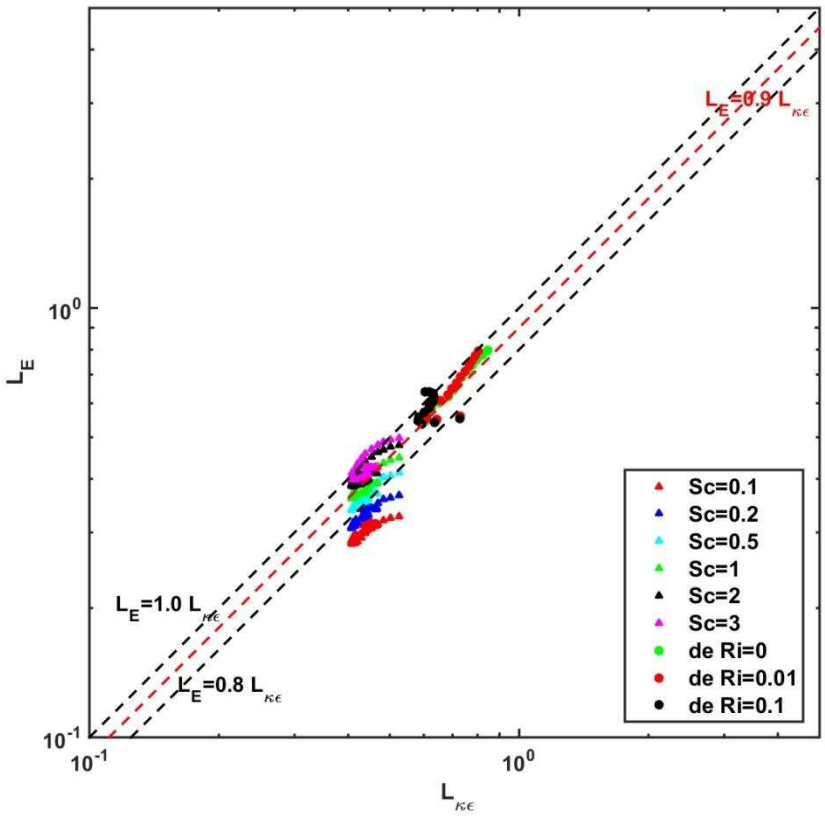

Figure 3.25: Comparison of L_E & $L_{k\varepsilon}$ for passive scalars in unstratified flows.

With these new findings, a revised model for the diascalar diffusivity can be derived by recasting L_E and T_L in terms of L_T and $L_{k\varepsilon}$. The resulting new model is given as

$$K_S = 1.1\ \gamma'\ L_T\ k^{1/2}, \tag{3.13}$$

The new model is clearly more practical since it relies entirely on large scale quantities i.e. L_T and *k* are both large scales quantities in a turbulent flow. In essence, Eq. (3.13) can be viewed as a turbulence closure scheme in the spirit of turbulence modeling since it does not rely on any small-scale turbulence quantity for closure.

As a final step of this modelling exercise, the diascalar diffusivity computed using new model, Eq. (3.13) and exact diascalar diffusivity from DNS for unstratified flows are compared in Fig.3.26. Red continuous line indicates the 1:1 relationship between K_{model} and K_{exact}. 20% of

confidence intervals are indicated by dashed black lines. It can be seen that the proposed model does reasonably well in capturing the exact diffusivities.

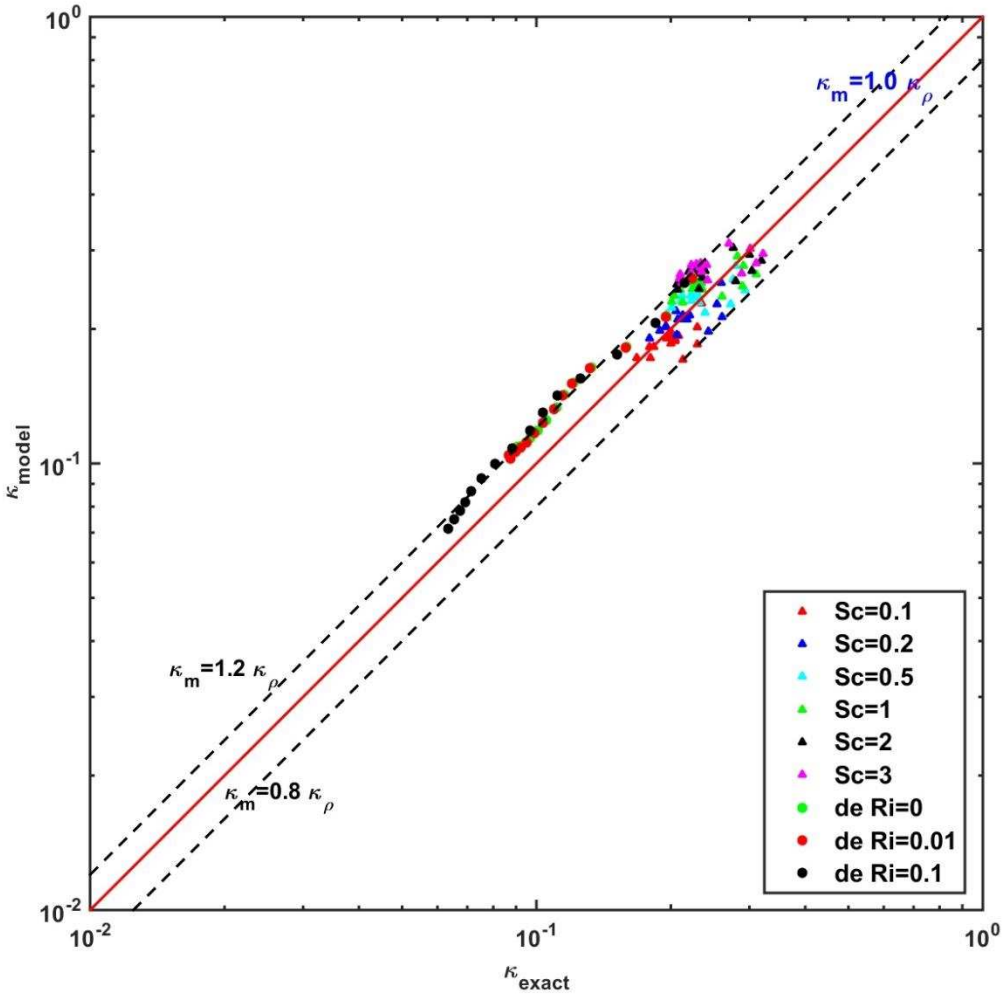

Figure 3.26: Comparison of diascalar diffusivity computed using model (K_{model}) given by Eq. (3.13) and DNS data (K_{exact}).

3.8 Conclusions

In this chapter, a detailed DNS study was performed to investigate turbulent mixing of passive scalars in an unstratified homogeneous turbulent flow. The main findings of this study are twofold: first, for turbulent flows, the mixing is not sensitive is found not to be sensitive to Schmidt number provided that there is sufficient separation of scales i.e. the diascalar diffusivities have to

at least one or more order of magnitude higher their molecular counterparts. Second, a revised model to the VS model which has considerable potential for practical applications was proposed and validated. In what follows in the next chapter, suitability of the new proposed model to stably stratified flows is considered.

CHAPTER 4

MIXING OF ACTIVE SCALARS

4.1 Introduction

Stably stratified flows are common in the environment flows such as oceans, lakes and the atmosphere. Stable stratification arises from temperature and/or salinity variations in deep water environments where the mean potential density increases with depth. In a stably stratified fluid, the heavier fluid lies below the lighter fluid. Dynamically, the presence of a stable stratification has substantial effect on physical processes such as turbulent scalar mixing. Accurate prediction of turbulent mixing in such flows is important for many applications such as pollutant dispersion in air and water bodies, weather and climate prediction. As such, in this study, the main focus is on parameterization of active scalar mixing.

In what follows in this chapter, first a formal problem statement is stated in Sec. 4.2 which is followed by a description of the DNS data in Sec. 4.3. The main results on the modeling aspects of the study are presented in Sec. 4.4.

4.2 Problem statement

The main goal in this Chapter is to test and refine the diascalar diffusivity parameterization that was developed in Chapter 3 for passive scalars to active scalar mixing in stably stratified flows at low, moderate and high stratification. Specifically, the key questions are: “Does the diascalar diffusivity model proposed in Chapter 3 as $K_S = 1.1\,\gamma'\,L_T\,k^{1/2}$ for passive scalar mixing in unstratified flows seamlessly extend to active scalar mixing in stably stratified flows? If not, what modifications are required to account for the buoyancy effects in the model?

4.3 DNS formulation

DNS is an exact numerical solution (within numerical accuracy of the computational schemes) of the Navier-Stokes (N-S) equations that is obtained by resolving all scales of motion in a given turbulent flow. First theorized by John Von Neumann in 1949 (Davidson, 2004), DNS is the simplest form of numerical simulations that does not resort to the use of turbulence models. To resolve all scales of motion, the grid size must be of the order of the Kolmogorov length scales L_η while the domain length L must be large enough to capture the largest energy containing eddies (Pope, 2000).

Orszag & Patterson (1972) pioneered the pseudo-spectral computational method. The pseudo spectral DNS code used in a previous study of stably stratified turbulence from which the data for the present study is obtained is based on the methodology put forth by Orszag and Patterson (1972). The serial code was written in the FORTRAN 77 programming language. The DNS data used in this chapter were obtained from the study by Schaad (2012) for his MS thesis research. His simulations were conducted for stably stratified decaying turbulent flow with low, moderate and high stratification.

DNS data from simulations of stratified decaying flow for Prandtl (or Schmidt) number Pr=1 is used for a range of Richardson numbers, which is a non-dimensional number that indicates strength of the stratification. Seven different simulations were done by Schaad (2012) with initial Richardson numbers Ri = 0, 0.01, 0.1, 0.4, 1.6, 10, 40 and 158 that encompass flows ranging from low to moderate to strong stratification with an initial turbulent Reynolds number Re=625. It must be noted that these simulations were unforced and hence the flow decayed with time dues to the absence of an energy input source beyond the initial input at the start of the simulations. The N-S solutions were computed such that the lowest wavenumber κ_0 =2, which implies that the

computational domain had a length $L=\pi$. Periodic boundary conditions were applied to the cubic box with a grid resolution of 256^3 grid points.

4.4 Modeling of turbulent scalar mixing in stably stratified flows

The first step is to assess how well the proposed model given by $K_S = 1.1\ \gamma'\ L_T\ k^{1/2}$ using the stably stratified DNS data. The model prediction of the diffusivity is plotted again the exact diffusivity for all *Ri* cases including the unstratified decaying simulation (denoted by *Ri* =0) as shown in Fig. 4.1. It is evident that as the stratification increases (i.e. beyond *Ri* = 0.39), the model overpredicts the diffusivity. This implies that as buoyancy effects become significant and dominate the flow, the diascalar diffusivity is suppressed and the inherent physics in the proposed model does not fully account for this effect. Clearly, further analysis is required to correct for this effect.

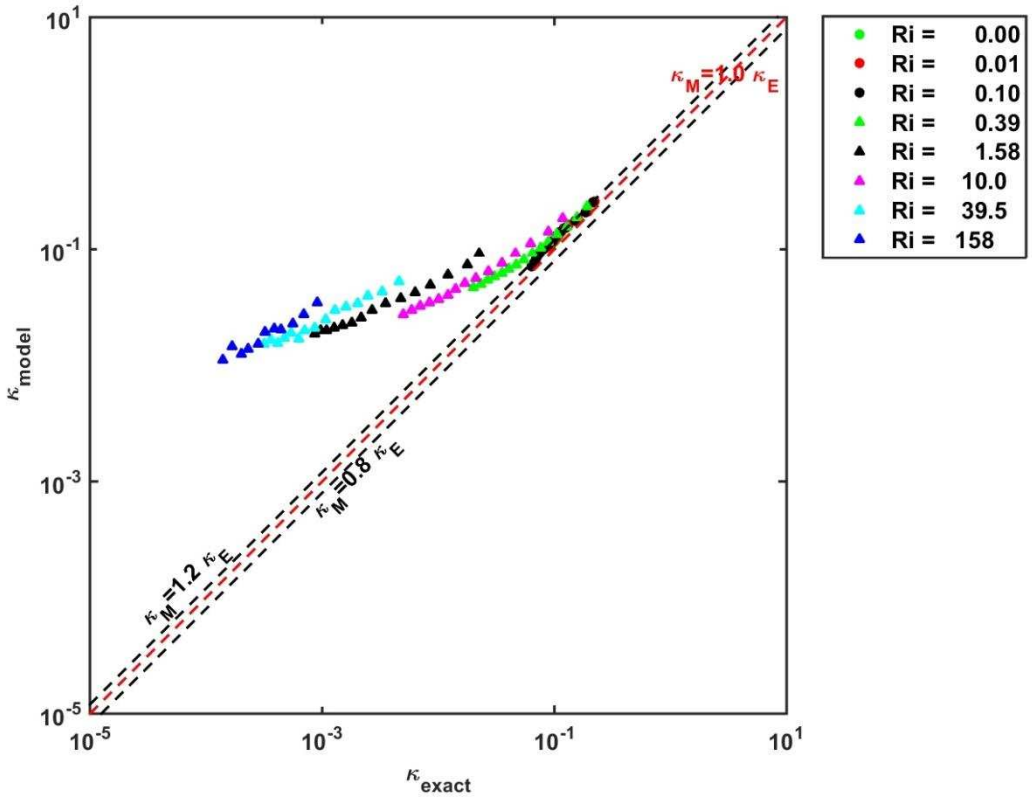

Figure 4.1: Model diffusivity versus exact diffusivity using DNS data of stably stratified flows.

Given that the correlation between the Ellison and Thorpe length scales have been previously established by other researchers (see Itsweire et al. 1993, Mater et al. 2013), it is unlikely that the differences are related to the breakdown in this relationship. Regardless, before proceeding to other possibilities, this relationship is tested again as shown in Fig. 4.2. It is clear that $L_T = 0.8\ L_E$ still holds across a broad range of stratification.

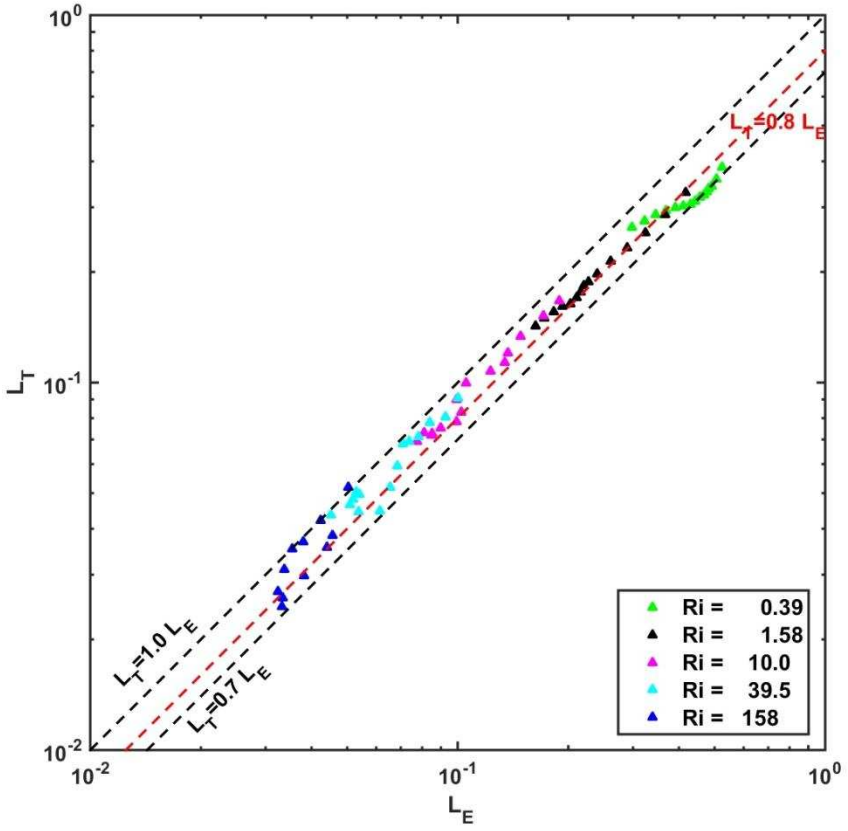

Figure 4.2: Comparison between Ellison and Thorpe length scales for stably stratified flows.

The next step is to reconfirm whether the original model proposed by Venayagamoorthy and Stretch (2006, hereafter the VS model) holds for the diascalar diffusivity (previously discussed in Chapter 3 in Sec. 3.7). Fig.4.3 shows a plot of the nondimensional diascalar diffusivity versus the turbulent Peclet number for all *Ri* cases. It is evident that the VS model continues to capture the exact diffusivity reasonably well. The parameter γ' is computed for these active scalar mixing

simulations in decaying stably stratified flows and shown as a function of eddy turnover time in Fig.4.4 for different stratifications. Even though high fluctuations in the value are evident at high *Ri* (due to the occurrence of linear internal wave motions), average values for γ' are closer to 0.7. However, as previously discussed in Sec. 3.7 of Chapter 3, the need for a practical model that utilizes only large scale turbulent flow quantities dictates that an improvement to the current proposed model is required.

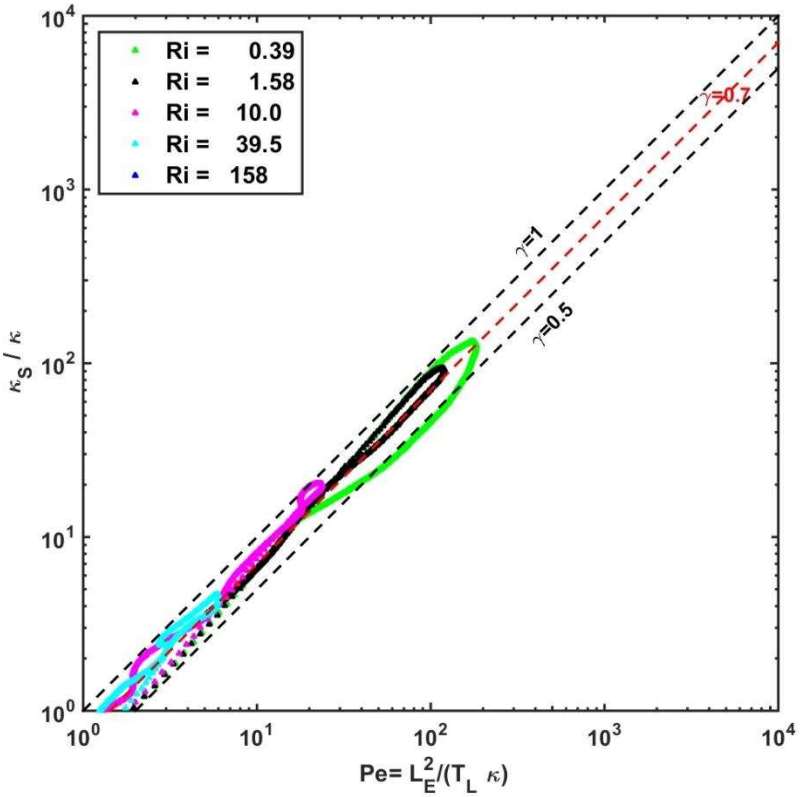

Figure 4.3: Non-dimensional diapycnal diffusivity with turbulent Peclet number for different decaying stratified flow. Dashed black lines represents γ'=1 and 0.5.

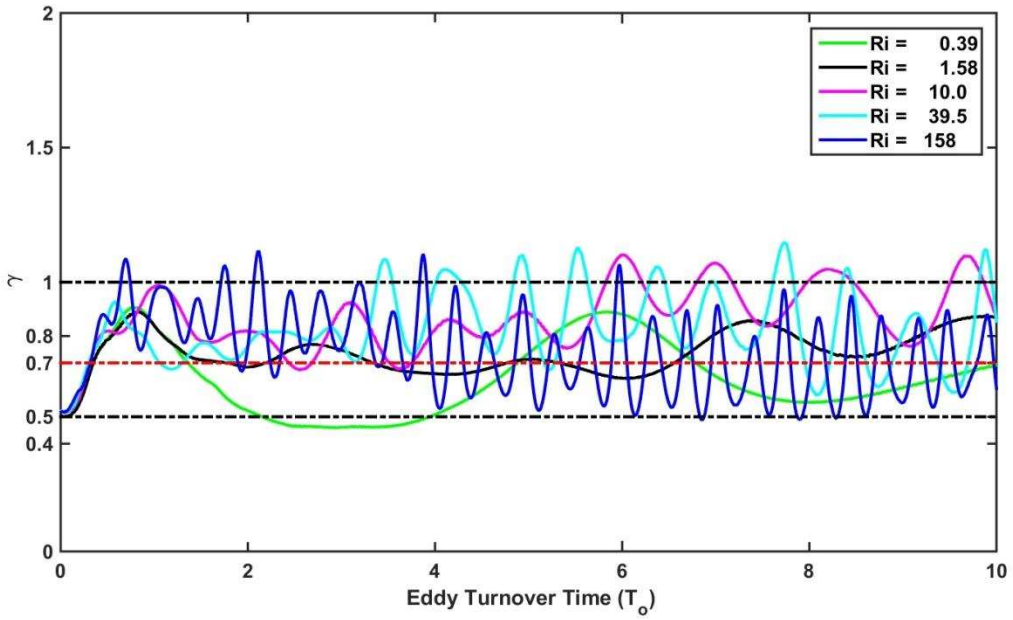

Figure 4.4: Values for γ' plotted with eddy turnover time for different stratifications. Dashed black lines represents γ'=1 and 0.5.

Returning to the proposed model given by $K_S = 1.1\,\gamma'\,L_T\,k^{1/2}$, the next check point pertains to the linear relationship that was shown to hold between the turbulent kinetic energy length scale $L_{k\varepsilon}$ and L_E for unstratified flows in Chapter 3 (see Sec. 3.7). A plot of L_E versus L_E is shown in Fig. 4.5. Clearly, as stratification increases, the linear relationship between these two length scales no longer holds, especially beyond Ri = 0.4, which can be considered to be a somewhat mildly stratified flow case. Physically, this breakdown can be attributed to the strong anisotropy that develops in the flow due buoyancy effects as *Ri* increases. As the buoyancy effects increases, the vertical fluctuations decrease constraining the vertical motions of fluid particles thus resulting in much diminished values of L_E. On the other hand, $L_{k\varepsilon}$ is based on the turbulent kinetic energy which is based on the three-dimensional velocity fluctuations. Hence, it continues to stay large.

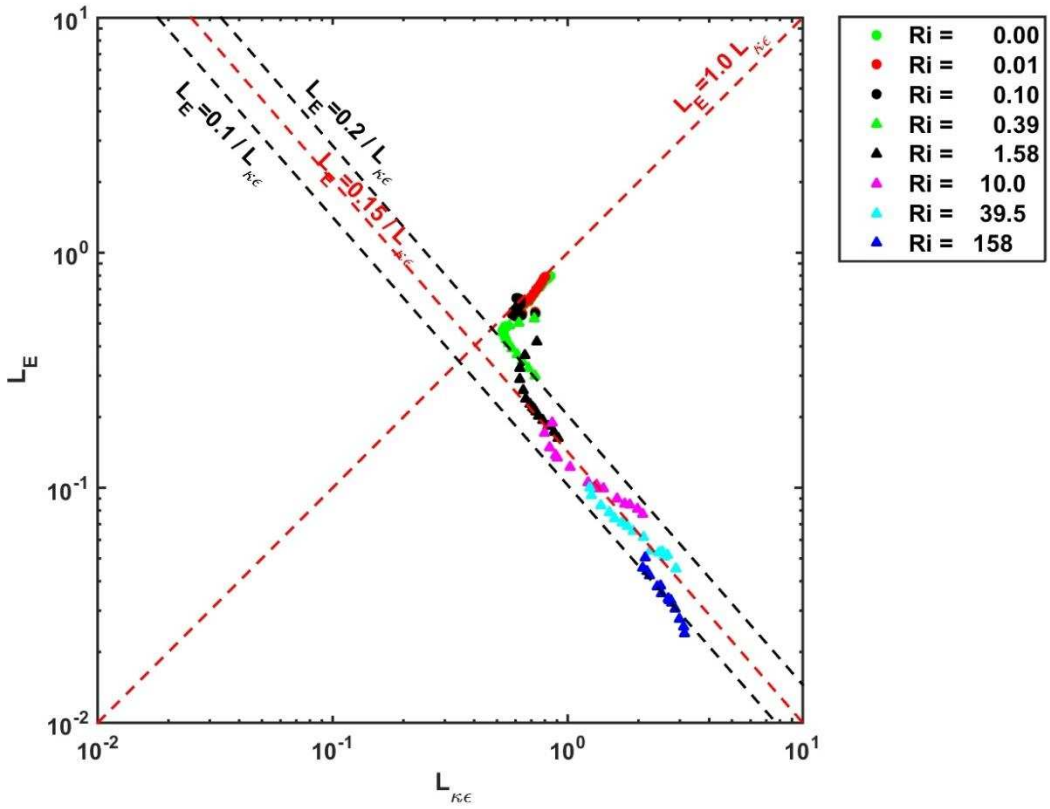

Figure 4.5: Ellison length scale versus turbulent kinetic energy length scale for low, moderate and high stratification.

What can also be seen in Fig.4.5 is an inverse trend in the relationship between L_E and $L_{k\varepsilon}$ for Ri $\geq$ 0.4. This trend is closely captured by $L_E = 0.15\, L_{k\varepsilon}$. Fig. 4.6 shows that a constant of 0.15 is a suitable proportionality constant.

Using this modified relationship between L_E and $L_{k\varepsilon}$ for the moderate to strong stably stratified flow cases, the diffusivity can be modified accordingly.

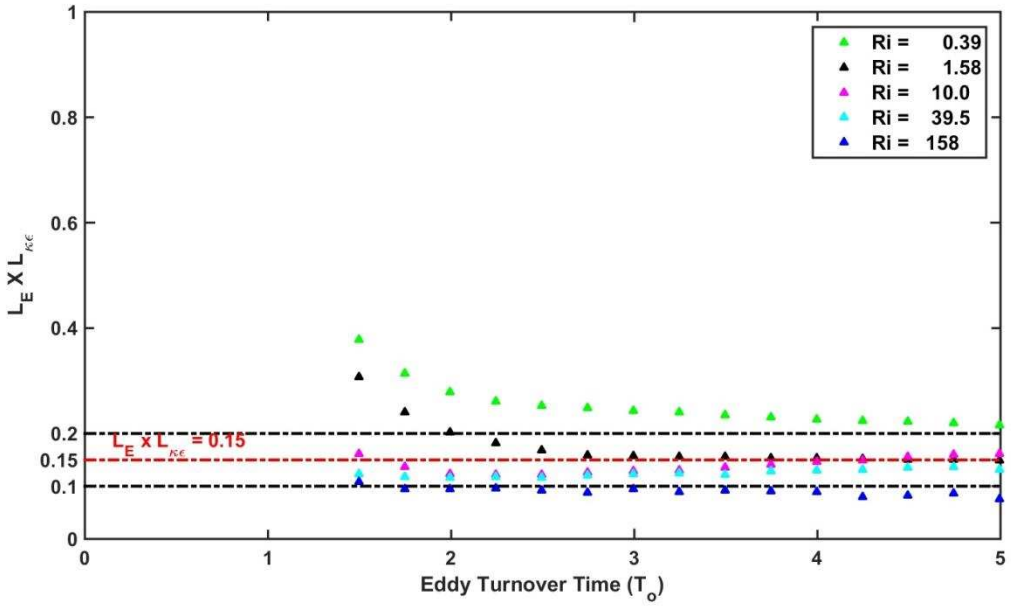

Figure 4.6: Inverse relationship between Ellison and kinetic energy length scales for different stratification.

Beginning with the VS model for the scalar diffusivity given by

$$K_S = \gamma' \frac{{L_E}^2}{T_L},$$

first, L_E can be substituted with $L_T/0.8$ and T_L can be rewritten as $L_{k\varepsilon}/k^{1/2}$. Thus,

$$K_S = \gamma' \frac{\left({L_T}/{0.8}\right)^2}{L_{k\varepsilon}/k^{1/2}}.$$

Now $L_{k\varepsilon}$ can be replaced by $0.15/L_E$ which in conjunction with the relation between L_E and L_T can further simplified as $L_{k\varepsilon} = (0.15 * 0.8)/L_T$ to provide a model for the scalar diffusivity as

$$K_S = \gamma' \frac{\left({L_T}/{0.8}\right)^2}{(0.15 * 0.8)/L_T} k^{1/2},$$

which simplifies to

$$K_d = 13\, \gamma'\, {L_T}^3\, k^{1/2}, \tag{4.1}$$

It must be noted that the model presented in Eq. (4.1) might appear at first sight to be dimensionally inconsistent due to the inverse relationship between the relevant length scales it should provide a good quantitative estimate of the diascalar diffusivity.

The diascalar diffusivity computed using revised model, Eq.4.1 and exact scalar diffusivity using DNS data for active scalars in stably stratified flows shown in Fig.4.7. Red continuous line indicates the 1:1 relationship ($K_{model} = K_{exact}$). 20% of confidence intervals are indicated by dashed black lines. It can be seen that there is a significant improvement in the prediction compared to that shown in Fig. 4.1 using the passive scalar model.

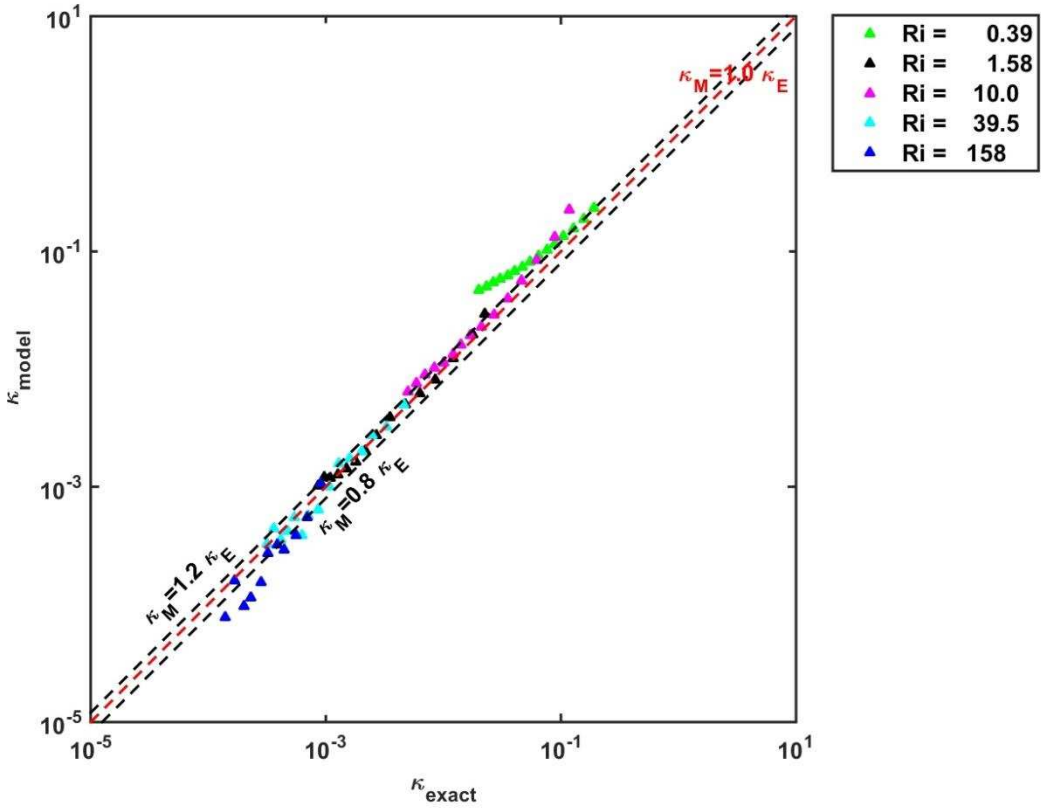

Figure 4.7: Comparison of Scalar diffusivity computed using model (K_{model}) and DNS data (K_{exact}) for active scalar in stratified flow.

As a final summary plot, predictions of diffusivities using both the passive scalar model as well as the active scalar model are shown against exact diffusivities for all the available DNS data

for forced unstratified flows and decaying stratified flows in Fig.4.8. To construct this plot, the two relevant models are applied to their appropriate regimes, respectively. The model $K_S = 1.1\,\gamma'\,L_T\,k^{1/2}$is used for passive scalar mixing as well as for mildly stratified flows, while the model $K_d = 13\,\gamma'\,{L_T}^3\,k^{1/2}$ is used for the moderate to strongly stably stratified flows.

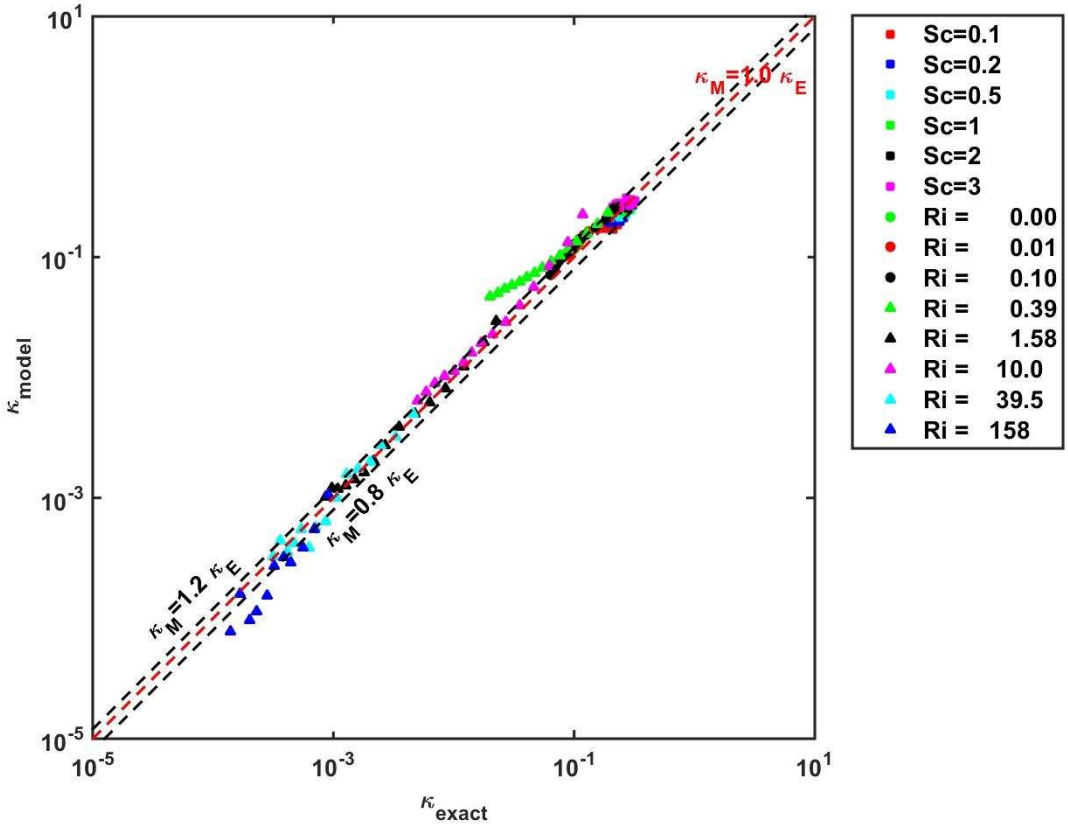

Figure 4.8: Master plot showing the diffusivity models for both passive and active scalars in unstratified and stratified flows.

CHAPTER 5

CONCLUSION

5.1 Summary of studies

The main focus of the work presented in this thesis revolves around mixing of passive and active scalars in turbulent flows. DNS was used to simulate scalar mixing in homogeneous unstratified and stably stratified turbulent flows. For unstratified flows, the effect of varying Schmidt numbers on turbulent mixing was investigated in Chapter 3. A total of 6 different simulations were performed for $0.1 \leq Sc \leq 3$. Quantitative and qualitative analysis were presented to highlight the mixing under for varying *Sc*. The highlight of the study presented in Chapter 3 focused on a new model for quantifying the diascalar diffusivity that used a model proposed by Venayagamoorthy and Stretch (2006) as its basis.

In Chapter 4, DNS data for different stratified flows with Prandtl number Pr=1 obtained from the work by Schaad (2012) were used to study the active scalar mixing in stably stratified turbulence. The main thrust of this study was to investigate the suitability and required modification (if any) of the new proposed model for diascalar diffusivity in Chapter 3 for stably stratified flows

The main conclusions from Chapter 3 and 4 are summarized in Sec.5.2 and recommendations for future work on further developments of the scalar mixing model are provided in Sec.5.3.

5.2 Conclusions from chapter 3 and chapter 4

In Chapter 3, a DNS parametric study was performed for different Schmidt numbers *Sc*=0.1, 0.2, 0.5, 1, 2 and 3 in forced unstratified homogeneous turbulent flow. The forcing scheme was added in order to achieve stationary velocity fields. A careful analysis was carried to ensure that numerical resolution issues were adequately addressed before embarking on a detailed study to investigate the flow physics. Results of energetics, statistics of the scalar field and coherent structures were presented to show the characteristics of the flow and scalar fields. It was found that the scalar dissipation rate which essentially characterizes mixing was not so sensitive to the molecular diffusivity. This was clearly demonstrated by plotting the non-dimensional diascalar diffusivity versus the turbulent Peclet number (see Fig. 3.26). It was observed that diascalar diffusivity can be predicted by the VS model.

The main highlight of this research was the development of an improved model to the VS model that utilizes the well-known Thorpe length scale in oceanography as well as the turbulent kinetic energy as a suitable velocity scale to parameterize the turbulent diascalar diffusivity as $K_S = 1.13\,\gamma'\,L_T\,k^{1/2}$ in homogeneous unstratified flows. In Chapter 4, the above expression was modified to account for anisotropy effects. In short, an inverse relationship between Ellison L_E and kinetic energy length scale $L_{k\varepsilon}$ was found as $L_{k\varepsilon} = 0.15/L_E$. Hence, a modified model was proposed as $K_d = 13\,\gamma'\,{L_T}^3\,k^{1/2}$ for active scalars in homogeneous stratified flow. A priori tests using DNS data show remarkable promise in the ability of the proposed models to capture the exact turbulent diffusivities.

5.3 Suggestions for future research

As with most DNS studies, a major limitation of the present study is the low Reynolds numbers achieved in simulations. The code that was used for this study is serial and thus simulations with 256^3 grid points take about a week of clock time to run for simulating 3 eddy turn over times. Simulations should be conducted at much higher resolutions in order to achieve higher turbulent Reynolds numbers to further test the relationships and models that have been proposed here. Another avenue is to obtain DNS data at high turbulent Reynolds numbers for stratified and unstratified flows from other researchers to validate the proposed scalar diffusivity model. This option is desirable since it will allow for independent verification of the model proposed in this study.

Another important missing ingredient in the flows studied in this work is the lack of mean shear in the flow field. Most natural turbulent flows are sustained by mean shear generated from proximity to boundaries or differential flow. The robustness of the proposed model should be tested with simulations that are forced by mean shear. Another important missing piece is the use of an experimental study to validate the proposed model. An experiment study on passive scalar mixing in a fully developed channel flow or in a mixing tank (stirred by rotation) would be provided for a useful practical comparison.

As a final summary, it must be noted that the models proposed in this study require further (extensive) testing under higher Reynolds number flow conditions. If shown to be valid, they would be widely useful for quantifying turbulent mixing using field measurements of large scale quantities (i.e. L_T and k) as well as serve as a simple and improved turbulence closure scheme.

REFERENCES

Bogucki D., Domaradzki J. A. and Yeung P.K. (1997). Direct numerical simulations of passive scalars with Pr>1 advected by turbulent flow. *Journal of Fluid Mechanics*.

Eswaran V. and Pope S.B. (1988). An examination of forcing in Direct Numerical Simulations of turbulence. *Computers & Fluids*, vol.16,No.3, 257-278.

Eswaran V. and Pope S.B. (1987). Direct numerical simulations of the turbulent mixing of a passive scalar. *Physics of Fluids*.

Gotoh T. and Yeung P. K. (2013). Passive scalar transport in turbulence: A compuatational perspective. In K. Y. Davidson P. A., *Ten chapters in turbulence* (pp. 87-131). Cambridge University press.

Gotoh T., Fukayama D. and Nakano T. (2002). Velocity field statics in homogeneous steady turbulence obtained using a high resolution direct numerical simulation. *Physics of Fluids*.

Hanazaki H., Konishi K. and Okamura T. (2009). Schmidt-number effects on the flow past a sphere moving vertically in a stratified diffusive fluid. *Physics of Fluids*.

Itsweire E. C., Koseff J. R., Briggs D. A. and Ferziger J. H. (1992). Turbulence is stratified shear flows: Implications for interpreting shear-induced mixing in the ocean. *Journal of Physical Oceanography*.

Mater B. D., Schaad S. M. and Venayagamoorthy S. K. (2013). Relevance of the Thorpe length scale in stably stratified turbulence. *Physics of Fluids*.

Overholt M. R. and Pope S.B. (1996). Direct numerical simulation of a passive scalar with imposed mean gradient in isotropic turbulence. *Physics of Fluids*.

Pope S. B. (2000). *Turbulent Flows.* cambridge,UK: Canbridge University press.

Schaad S. M. (2012). *Dynamics and structure of stably stratified turbulence.* Colorado State University.

Sreenivasan, K. R. (1995). The passive scalar spectrum and the Obukhov-Corrsin constant. *Physics of Fluids*.

Stretch D. D. and Venayagamoorthy S. K. (2010). Diapycnal diffusivities in homogeneous stratified turbulence. *Geophysical Research Letters*.

Venayagamoorthy S. K. and Stretch D. D. (2010). On the turbulent Prandtl number in homogeneous stably stratified turbulence. *Journal of Fluid Mechanics*, vol.644, 359-369.

Venayagamoorthy S. K. (2002). *Turbulent mixing and dispersion in environmental flows.* Durban, South Africa: University of Natal.

Venayagamoorthy S. K. and Stretch D. D. (2006). Lagrangian mixing in decaying stably startified turbulence. *Journal of Fluid Mechanics*.

Venayagamoorthy S. K. and Stretch D. D. (2009). On the turbulent Prandtl number in homogeneous stably startified turbulence. *Journal of Fluid Mechanics*.

Warhaft Z. (2000). Passive scalars in turbulent flows. *Annual Reviews of Fluid Mechanics*, 32: 203-240.

Yeung P. K. and Pope S. B. (1992). Differential diffusion of passive scalars in stationary isotropic turbulence. *Thirteenth Symposium on Turbulence.* Rolla: University of Missouri.

Yeung P. K., Shuyi Xu and Sreenivasan K. R. (2002). Schmidt number effects on turbulent transport with uniform mean scalar gradient. *Physics of Fluids*.

Yeung P.K. and Pope S.B. (1993). Differential diffusion of passive scalars in isotropic turbulence. *Physics of Fluids*.

Yeung P.K., Donzis D. A. and Sreenivasan K. R. (2005). High-Reynolds-number simulation of turbulent mixing. *Physics of Fluids*.